Finding the stable structures of $N_{1-x}W_x$ with an *ab initio* high-throughput approach

Michael J. Mehl*
Center for Computational Materials Science, Naval Research Laboratory, Washington, DC 20375, USA

Daniel Finkenstadt and Christian Dane
Department of Physics, U.S. Naval Academy, Annapolis, Maryland 21402, USA

Gus L. W. Hart
Department of Physics and Astronomy, Brigham Young University, Provo, Utah 84602, USA

Stefano Curtarolo†
Materials Science, Electrical Engineering, Physics and Chemistry, Duke University, Durham, North Carolina 27708, USA
(Received 31 January 2014; revised manuscript received 20 April 2015; published 26 May 2015)

Using density functional theory calculations, many researchers have predicted that various tungsten nitride compounds $N_{1-x}W_x$ ($x < \frac{1}{2}$) will be "ultraincompressible" or "superhard," i.e., as hard as or harder than diamond. Necessary conditions for such compounds are that they have large bulk and shear moduli, greater than approximately 200 GPa, and are elastically and vibrationally stable. Compounds with such desirable properties also must be energetically stable against decomposition into other compounds. This test for stability can only be found after the determination of the convex hull for $N_{1-x}W_x$, which connects the lowest enthalpy structures as a function of composition. Unfortunately, the experimental phase diagram of the N-W structure is uncertain, as it is difficult to break the N_2 bond to form compounds with tungsten. Experiment also indicates that there are a large number of partially filled sites in most N-W structures. This introduces computational difficulties since we cannot easily model randomly placed vacancies. In addition, van der Waals forces play a significant role in determining the structure of solid N_2 and the nitrogen-rich compounds. This makes it difficult to determine the relative energies of these compounds, as there is no universally accepted density functional incorporating van der Waals interactions. The exact shape and even composition of the convex hull is dependent upon the choice of density functional, even if we only chose between the local density approximation and a generalized gradient functional. Despite these difficulties, computations can determine much about the ground-state form of the convex hull. Here, we use high-throughput calculations to map out the hull and other low-energy structures for the N-W system. The lowest-energy structures all have vacancies, on the tungsten sites in hexagonal-based compounds, and on both the nitrogen and tungsten sites in cubic compounds. We find that most of the N-W structures proposed in the literature, both theoretical and experimental, are above the convex hull, in some cases by over 0.2 eV/atom. One of the ground-state phases, N-W in the NbO structure, has relatively large bulk (>300 GPa) and (>200 GPa) shear moduli, and so is a candidate superhard material. This will require further investigation.

DOI: 10.1103/PhysRevB.91.184110 PACS number(s): 64.30.Ef, 64.70.kd, 61.50.Ah

I. INTRODUCTION

One of the major goals of electronic-structure calculations is the prediction of crystal structures as a function of composition [1–3]. Determining the possible configurations of a compound as a function of composition is the first step in determining its material properties at equilibrium. It is also likely that any pressure- or temperature-driven phase transitions will be from the equilibrium structure to another structure which is close to it in energy and composition. Such calculations are of particular interest when there is little known about the system theoretically.

There are a variety of mechanisms for this: searching over a wide range of known [4] and likely [5] structures for the material in question, searches starting from randomly positioned atoms [6], and even structures predicted from apparently "out of the blue" [7]. In the end these techniques produce a set of metastable structures, all of which have zero force on the atoms in the crystal, zero stress, and no imaginary phonon modes. Some structures will be stable, that is, it is not energetically favorable for them to decompose into into other structures.

When searching for stable structures, this last point is key. We can find the lowest-energy structure of, e.g., composition A_2B_5, but we cannot tell if it is truly stable until we show that it cannot decompose into 2A + 5B, or A_2B_2 + 3B, or some other combination of structures. In other words, to completely determine structural stability of a compound, we must search over all possible compositions.

Once this is done there is still the question of whether or not we have done the appropriate calculation. Most electronic-structure calculations are done using the Kohn-Sham *ansatz* [8] to density functional theory (DFT) [9]. Since the exact density functional is not known, we necessarily use approximate forms. It is not *a priori* certain that the local density approximation (LDA) [10,11] will give the same results as a generalized-gradient functional such as Perdew-Burke-Ernzerhof (PBE) [12]. If van der Waals forces

*michael.mehl@nrl.navy.mil
†stefano@duke.edu

are important, we should use some variety of van der Waals–enabled functional [13]. If multiple functionals for a given system predict the same stable structures and compositions, then it is likely that these compounds will form. If different functionals produce different results, then we cannot decide the issue on the basis of current density functional theory and must appeal to more accurate techniques or to experiment.

As an example, we look at tungsten nitrogen system. There are many experimental studies showing evidence of stable $N_{1-x}W_x$ compounds [14–21], and there is no assessed phase diagram diagram available [22]. Indeed, until recently [21] it was very difficult to make nitrogen-rich $N_{1-x}W_x$ compounds since tungsten does not dissolve appreciable amounts of N_2 [23]. In addition, above 600 °C the compound usually referred to as tungsten nitride decomposes to NW_2, which itself loses nitrogen above 1000 °C [23].

Tungsten carbide is of interest as a structural material, or at least a coating, because of computational studies which claim that some compounds $N_{1-x}W_x$ with $x < \frac{1}{2}$ are "superhard", or at least have very stiff elastic constants and so are superhard candidates [24–30].

While all these calculations show that the favored phase of $N_{1-x}W_x$ is stable against decomposition into N_2 and tungsten, none provide a detailed calculation of the possible stable and metastable structures of $N_{1-x}W_x$ as a function of tungsten concentration x. It is thus difficult to determine if these structures will form experimentally, or to determine if structures which do form are stable or only metastable.

Our original motivation for this study was the possibility that N_4W (or $N_{0.8}W_{0.2}$) might be a superhard metal [30] and can be in fact easily fabricated. As noted above, this requires knowledge of the entire equilibrium phase diagram for $N_{1-x}W_x$. We did this using AFLOW [31], a high-throughput front end for electronic-structure calculations [1]. AFLOW allows us to quickly examine a selected range of structures using high-performance supercomputers and modern density functional electronic-structure techniques. The AFLOW prototype database, which was originally used to describe intermetallic alloys [32–36], can easily be enlarged [37]. We were therefore able to include ionic and covalent structures for systems similar to N-W. These include borides, carbides, oxides, and other nitrides. We also invented many structures to mimic the random pattern of vacancies on both the tungsten and nitrogen sites that have been observed under experimental conditions.

AFLOW allows the use of a variety of different density functionals. We did our primary calculations using the Perdew-Burke-Ernzerhof (PBE) generalized-gradient functional [12]. For low-energy systems we also used the local density approximation [10,11] (LDA). We also approximated van der Waals forces, which are important in nitrogen-rich structures, using the vdW–DF2 functional [38]. As we shall see, predictions for ground-state structures are strongly dependent on the choice of functional.

Here, we are searching for structures of composition $N_{1-x}W_x$ which are stable, or are metastable with a reasonable probability of being found experimentally. A metastable compound must be vibrationally stable, i.e., have no imaginary phonon frequencies as well as elastic constants which satisfy the Born criteria [39]. True stability requires an additional step: consider the decomposition of a compound N_AW_B into the ground-state forms of its end-point components, αN_2 [40], and body-centered-cubic tungsten [41]. This decomposition requires a change in enthalpy

$$\Delta H(N_AW_B) = [E(N_AW_B) - B\,E(W) - (1/2)A\,E(\alpha N_2)]/(A+B) < 0, \quad (1)$$

where $\Delta H(N_AW_B)$ is the formation energy per atom of a compound with this stoichiometry, $E(N_AW_B)$ is the energy/formula unit of the compound, $E(W)$ is the equilibrium energy per atom of body-centered-cubic tungsten, and $E(\alpha N_2)$ is the equilibrium energy per molecule of solid αN_2. ΔH will be negative if it is energetically possible for the compound to be formed spontaneously from solid N_2 and W. The compound will be completely stable if it is not energetically favorable for it to decompose into any other N-W compound. This requires that the compound be on the convex hull determined from the plot of ΔH versus tungsten concentration $x = N/(M+N)$ over all possible compounds in the system [42].

The purpose of the paper is to determine ΔH for a sufficient number of N-W compounds so that we have a good approximation to the shape of the convex hull and the structures forming it, and to determine the electronic, elastic, and vibrational properties of compounds on or near the convex hull, looking for superhard candidates. An estimate of the actual hardness of these materials is beyond the scope of this paper, but in general will follow the procedures in Ref. [30].

The paper is organized as follows. Experimental and previous theoretical work is shown in Sec. II. Our computations are described in Sec. III. Our results are shown in Sec. IV, which is broken up into several subsections, including β (cubic) and δ (layered hexagonal) compounds, compounds containing N_2 dimers, compounds resembling SiO_2, and miscellaneous structures. Finally, we discuss our results in Sec. V.

Our study of tungsten nitride required searching over a large number of known experimental structures [43–47], and even inventing structures which had vacancy patterns related to those seen experimentally. The Supplemental Material [48] contains crystallographic information for 108 of the lowest-energy structures, along with additional computational details. In all, we studied over 500 structures using the high-throughput AFLOW platform. Structural parameters for these additional structures are available on request.

We always refer to the composition of tungsten nitride in the form $N_{1-x}W_x$, where x is the atomic fraction of tungsten, or, for stoichiometric compounds, N_AW_B, where A and B are integers. Various other authors reverse the order of these compounds, e.g., "r-W_2N_3" [21]. To avoid confusion, we place these designations in quotes. In the Supplemental Material [48], all structures are ordered by tungsten concentration x.

II. EXPERIMENTAL AND THEORETICAL BACKGROUND

Wriedt [22] summarizes the experimental N-W data known before 1990. The cubic β phase is essentially the face-centered-cubic NaCl structure (structure #67 in the Supplemental Material [48]), with vacancies on the nitrogen site leading to compounds of the form $N_{1-x}W_x$ with $x > \frac{1}{2}$. The cubic lattice constant for all of these phases is approximately

4.13 Å. These structures were originally studied by Hägg [14], and later by Khitrova and Pinsker [17–19]. Kiessling and co-workers [15,16] found a similar phase which they designated γ. This structure also seems to be related to the NaCl structure, but with $x \approx 1$.

The hexagonal δ phase structures were extensively studied by Khitrova and Pinsker [18,19]. They defined six distinct crystallographic structures $\delta_H^{I\text{-}IV}$ and $\delta_R^{V,IV}$, which we will discuss in more detail in the following. Compositions $N_{1-x}W_x$ are said to range from $x = 0.33$ to 0.67. As NaCl is the base structure for the β phase, we can consider tungsten carbide [49] (structure #61 in the Supplemental Material [48]) as the basis for most of the δ phase structures. These structures are composed of stacked triangular planes of tungsten or nitrogen atoms. Unlike the β phases, vacancies appear only in the tungsten planes.

In addition to bulk structures, Shen and Mai [50] have grown thin-film N-W films. They found some evidence of the β phase at NW_2, but most of the films were amorphous.

These compounds are difficult to make and to stabilize. As noted by Toth [23], "tungsten does not dissolve appreciable amounts of nitrogen as a terminal solid solution," and must be formed at temperatures under 800 °C. Recently, however, Wang, Yu, Lin *et al.* [21] (hereafter referred to as WYL+) were able to use solid-state ion exchange and nitrogen degassing under pressure to produce several tungsten nitride phases with compositions ranging from N_3W_2 to N_2W_3 ($0.4 \leqslant x \leqslant 0.6$). Although they do not state this, all of these structures can be classified as either β-NW or δ-NW, as defined above. We will have more to say about these structures as we discuss our computational results.

Computational studies of the tungsten-nitride system followed in the wake of the development of high-speed computers and computationally efficient density functional codes. We will discuss some of these papers in more detail in the next section. For now, we briefly describe their results. These researchers studied specific crystal structures of tungsten nitride, but none have examined structures over a large range of compositions.

Kroll, Schröter, and Peters [24] considered the nickel arsenide structure [51] (#59 in the Supplemental Material [48]) to be the ground state of NW. They also looked at several possible structures for N_2W, including baddeleyite [52] (#20), which they found to have the lowest energy, brookite [53] (#18), and cotunnite [54] (#23), which they found to be a high-pressure (>35 GPa) phase of N_2W.

Suetin, Shein, and Ivanovski [25] modeled tungsten nitride by assuming it to be in either the tungsten carbide (WC, #61 in the Supplemental Material [48]) or the sodium chloride (NaCl, #67) structure. They computed elastic constants, isotropic bulk moduli in the Reuss and Voigt approximations [55], and the corresponding isotropic Young's modulus and Poisson's ratio. The NaCl structure is elastically unstable, with $C_{44} < 0$. The WC compound, on the other hand, was found to be rather stiff, with a shear modulus of about 150 GPa. The enthalpy ΔH was not calculated, so there could be no estimate of stability against dissociation into N_2 and bcc tungsten.

Wang, Li, Li, Xu *et al.* [26] (hereafter WLLX+) used an evolutionary method to find two related N_2W structures (#11 and #12) which had shear moduli >200 GPa. These structures, which consisted of vertically aligned N_2 dimers alternating with hexagonal tungsten planes, have $\Delta H < 0$, as well as elastic constants satisfying the Born criteria [39]. In addition, both structures are insulators, with a band gap on the order of 1 eV.

Benhai, Chunlei, Xuanyu, Qiuju, and Dong [27] looked at the elastic behavior of a variety of NW ($x = \frac{1}{2}$) structures, at pressures up to 100 GPa. They found that the NiAs structure was preferred over the WC at all pressures. They did not calculate the change in enthalpy relative to the N_2 and bcc W end points, nor did they consider some of the lower-energy structures we report in the following.

Song and Wang [29] studied NW in the WC structure, N_2W in the $CoSb_2$ structure (#20, although they refer to it as IrP_2), and N_3W in the P_3Tc structure [56] (#10), using the LDA functional. The found a negative value of ΔH for all three compounds, although it is not clear what reference point they used for pure nitrogen. In all cases, they found shear moduli below 200 GPa but bulk moduli greater than 300 GPa.

Suetin, Shein, and Ivanovski [57] modeled N_2W in what we believe to be the CTi_2 structure [58], a cubic supercell of the NaCl structure with ordered vacancies on one of the sublattices (see structure #95 in the Supplemental Material [48]). This is an approximation to the cubic NW_2 phase found by Hägg [14]. Although they compared the electronic structure to that found for the WC and NaCl structures in their earlier paper [25], they give no information about the stability of this structure.

Du, Wang, and Lo [28] looked at a tetragonal analog (#26) to the hexagonal structures found by WLLX+. They found it to be stable compared to these structures above 150 GPa, but never stable compared to the cotunnite structure (#23). Li, Zhai, Fu *et al.* [59] computed the pressure dependence of the elastic constants of these structures, and found that both are elastically stable up to pressures of 200 GPa.

In addition to their experimental work, WYL+ [21] also used first-principles calculations to determine the elastic constants of the three stoichiometric structures they studied, as well as what they call the *c*-BN structure (actually zinc-blende [60–62] #65). Bulk moduli all exceed 350 GPa, and shear moduli are estimated at around 180 GPa, but reach 390 GPa for the *c*-BN structure. They did not otherwise discuss the possible stability of these phases.

Aydin, Ciftci, and Tatar [30] (hereafter ACT) modeled N_4W using the starting point of the ReP_4 structure [63] (#7). They found this structure to be mechanically stable, and $\Delta H < 0$. The shear modulus of this structure was approximately 200 GPa, and they estimated the hardness of the material to be on the order of *c*-BN. If it could be made, then, it would most likely be a superhard material. We will discuss our findings for this structure in detail in the following.

Zhang, Yan, Wei, and Wang [64] calculated the equilibrium lattice parameter and elastic constants of WYL+'s "*c*-W_3N_4" structure [21], which has the prototype [65] S_3U_4 (#47). Later Liu, Wang, Zhou, and Chang [66] looked at the pressure dependence of the elastic constants and phonon frequencies of the same structure. This structure has very large bulk and shear moduli, but we shall see that it is far above the convex hull of the tungsten nitride phase diagram.

Liu, Zhou, Gall, and Khare [67] recently computed the elastic constants of transition-metal nitrides in the NbO structure [68]. Their calculation for NW showed it to be very

stiff, with its bulk modulus over 300 GPa and the shear modulus above 200 GPa. We will discuss this structure further below.

Summarizing the experimental and theoretical results, we find that the low-lying structures of tungsten nitride fall into one of five classes, the first two roughly corresponding to structures discussed by Schönberg [49]:

(1) *β phases*. These structures are supercells of the cubic NaCl structure (#67 in the Supplementary Material [48]). Removing atoms from the supercells generally leads to a lower-energy cell. Examples are the S_3U_4 structures (#47 and #78), which have either one N or one W vacancy in an eight-atom supercell, the NbO [68] (#53) structure, which has second-neighbor N and W vacancies, and the CTi_2 structure [58] (#95), which approximates the NW_2 β phase found by Hägg [14]. For our purposes we will treat the similar γ-NW structure [15,16] as part of the β phase.

(2) *δ phases*. In general these are hexagonal or trigonal unit cells containing alternating triangular planes of nitrogen and tungsten. The tungsten planes generally contain vacancies [18,21]. The experimental composition of these phases ranges from about [21] N_4W_3 to NW_2 [18].

(3) *N_2 phases*. In these structures the N_2 molecules stay intact, possibly within a tungsten matrix. The only experimental examples we have of these phases are the several varieties of solid N_2 [40]. Computations have found structures with composition N_2W (Ref. [26], #11 and #12) and N_4W (Ref. [30], #7) that appear to be at least metastable.

(4) *SiO_2 phases*. These have not been seen experimentally, and are only exceptionally low in energy when using the vdW–DF2 van der Waals functional. In these structures, the nitrogen atoms form a tetrahedron around each tungsten atom, and each nitrogen bonds with two tungsten atoms. A number of such structures appear in the literature [69]. Here, we examine a few of the more common ones.

(5) *Miscellaneous structures*. This category includes those structures which do not fit into one of the categories defined above, including a derivative of the FeB_4 compound proposed by Van der Geest and Kolmogorov [70] (#8), and the surprisingly low-energy MoS_2 structure (#89). None of these have been seen experimentally.

III. METHODS

We began our search for the convex hull of the N-W system by using AFLOW [1,31,71] to quickly and efficiently search through a large database of structures. As the original AFLOW prototype database was for binary metallic alloys [32–36], we have extended it to include over 100 new structures. These include nitrides, oxides, borides, and carbides, as well as supercells of standard structures with atoms removed to mimic the random patter of vacancies seen experimentally. The crystallographic information for the important structures, including all of those discussed in Secs. II and IV are described in the Supplemental Material [48].

Electronic-structure calculations were done using the Vienna *ab initio* simulation package (VASP) [72,73], including core-state effects via the VASP implementation [74] of the projector augmented-wave (PAW) method [75].

AFLOW's default is to use the Perdew-Burke-Ernzerhof (PBE) implementation [12] of the generalized-gradient approximation (GGA) to density functional theory (DFT) [8,9]. There are, however, substantial differences, especially in the estimates of enthalpy changes, between PBE results and those from the LDA [10,11]. This was shown by WLLX+ [26], and we shall see further examples in the following. Accordingly, we calculated the convex hull using both LDA and PBE functionals within VASP.

Molecular nitrogen, ground state [40] αN_2 (#1 or #2 in the Supplemental Material [48]), is a van der Waals solid [76], and neither the LDA nor the PBE-GGA correctly predict its lattice constant. We studied the effect of van der Waals forces by utilizing the VASP implementation [13,77] of the vdW-DF2 functional [38] This functional was developed to handle the van der Waals interaction in general geometries, so we apply it over the entire range of compositions, calculating a third convex hull and phase diagram.

We used the VASP-supplied LDA and PBE PAW potentials for nitrogen and tungsten (specifically, May 2000 LDA and April 2002 PBE PAW potentials for N, and the July 1998 LDA and September 2000 tungsten W_pv PAWs). All calculations use a kinetic energy cutoff of 560 eV, which is 40% larger than the suggested cutoff for nitrogen (400 eV). Unless otherwise stated, we let the AFLOW package determine the k-point mesh for each structure. This is usually set to use approximately the same density of k points in reciprocal space for all structures.

Since there are a wide variety of structures in this system, both metallic and insulating, we made sure that the k-point mesh was dense enough to determine the electronic-structure energy to better than 1 meV/atom. For the NaCl structure, e.g., a $15 \times 15 \times 15$ Monkhorst-Pack grid [78] was originally used. For Wang *et al.*'s $P\bar{6}m2$ N_2W structure, we used a $15 \times 15 \times 9$ mesh.

In the initial VASP calculations performed via AFLOW, all structures are considered to be spin polarized, but the starting magnetization vanished as self-consistency was reached. The final calculations were all done assuming no moment.

The MedeA® software system [79] was used to drive VASP in calculations of the phonon spectra and for some other calculations. Elastic constants were computed by taking finite strains [80,81] and determining the slope of the corresponding stress-strain curve (as implemented in the MedeA® package, or using the native VASP option). Phonon frequencies were determined via the frozen-phonon approximation using the MedeA® package.

IV. COMPUTATIONAL RESULTS

The surprising thing about our computational work is that so little of it agrees with either the experimental or theoretical work discussed above. This section details our results, using three different density functionals. In the next section, we will discuss the disagreement between these results and previous work.

We computed the enthalpy of formation ΔH [Eq. (1)] for over 500 $N_{1-x}W_x$ structures using the AFLOW mechanism for high-throughput calculations, with VASP as our computational engine [72,73,82]. We used the PBE density functional [12] as our screening tool, but for "interesting" structures, i.e., structures within approximately 0.2 eV of the tie line, we also looked for the minimum energy structure using the LDA

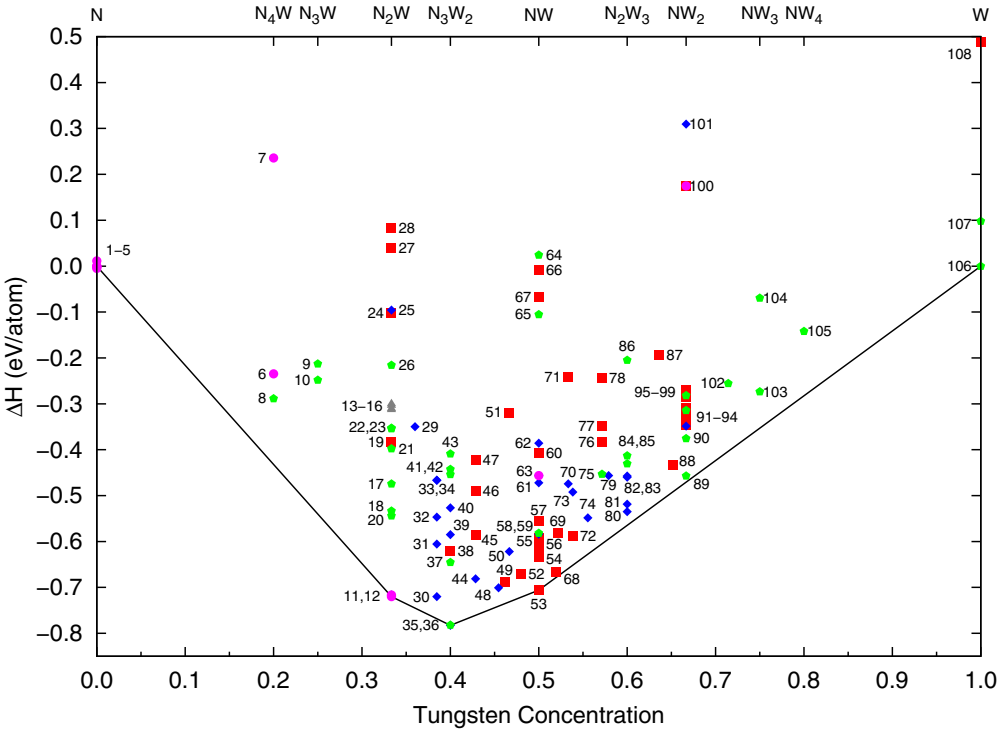

FIG. 1. (Color online) The relative enthalpy (1) of $N_{1-x}W_x$ for the 108 structures listed in the Supplemental Material plotted versus increasing tungsten concentration. These points were calculated using the local density approximation (LDA) with VASP. Red squares mark the β-phase structures, dark blue diamonds the δ phases, purple circles the N_2 (nitrogen dimer) phases, gray triangles the SiO_2 phases, and green pentagons the remaining miscellaneous phases. The labels correspond to the numbers of the structures in the Supplemental Material [48].

[10,11] and vdW–DF2 [38] functionals. We also included all of the stoichiometric structures, both experimental and theoretical, from Sec. II. In the case of experimental structures with randomly ordered vacancies, we constructed supercells of the base structure, removing nitrogen and/or tungsten atoms as needed to reach the desired composition. This resulted in many high-energy structures which we will not describe further, but the procedure also found structures which shape the convex hull of the energy diagrams.

The resulting phase diagrams for these 108 structures are shown in Figs. 1 (LDA functional), 2 (PBE functional), and 3 (vdW–DF2 functional). The diagrams are decidedly different, especially for tungsten concentrations $x < 0.4$. The shape, depth, and even composition of the convex hull changes as we move from LDA to PBE to vdW–DF2 functionals. Differences between functionals will be discussed in the comments on the individual structures, below.

In the following, we describe in detail the most interesting of the 108 structures listed in the Supplemental Material [48], paying particular attention to how our predictions change with change in the choice of density functional.

A. End points of the phase diagram

First consider the end-point structures: The lowest-energy N_2 structures are described by Donohue [40] and Mills, Oligner, and Cromer [83], comprising structures #1–#5 in the Supplemental Material [48] tables. We ignore the higher-energy nonmolecular structures of nitrogen such as cg-N [84], considering only solid N_2 crystals, where the molecules are bound by their mutual van der Waals attraction [76]. Since LDA and PBE do not explicitly include long-range van der Waals forces, we might expect some difficulty in describing the ground state.

Table I shows the calculation of the equilibrium structure of αN_2 in the $Pa\bar{3}$ structure, which is one of two proposed structures. The equilibrium lattice constant and bulk modulus were determined by fitting energy versus volume data to a third-order Birch fit [86] and the internal parameter x was determined by minimizing the forces on the atoms at fixed lattice constant [87]. While all three functionals correctly determine the N_2 bond length at 1.10 Å, none does particularly well in determining the equilibrium lattice constant and bulk modulus.

All N_2 structures are essentially degenerate, differing by no more than 0.03 eV per atom as we go from αN_2 to ϵN_2. Thus current versions of DFT and electronic-structure algorithms, even including van der Waals interactions, cannot accurately determine the ground state of N_2. We will study this in more depth in a future paper, but for now we will simply note that DFT calculations for pure nitrogen, and presumably for nitrogen-rich compounds, differ considerably depending on the choice of functional. One consequence of this is that the minimum entropy for this system ranges from −0.35 to −0.75 ev/atom, depending on the choice of functional.

Tungsten is naturally found in two forms [41], α−W (#106), the ground-state body-centered-cubic structure, and β-W (#107), commonly referred to by its *Strukturbericht* [43] designation A15. For this calculation we also considered

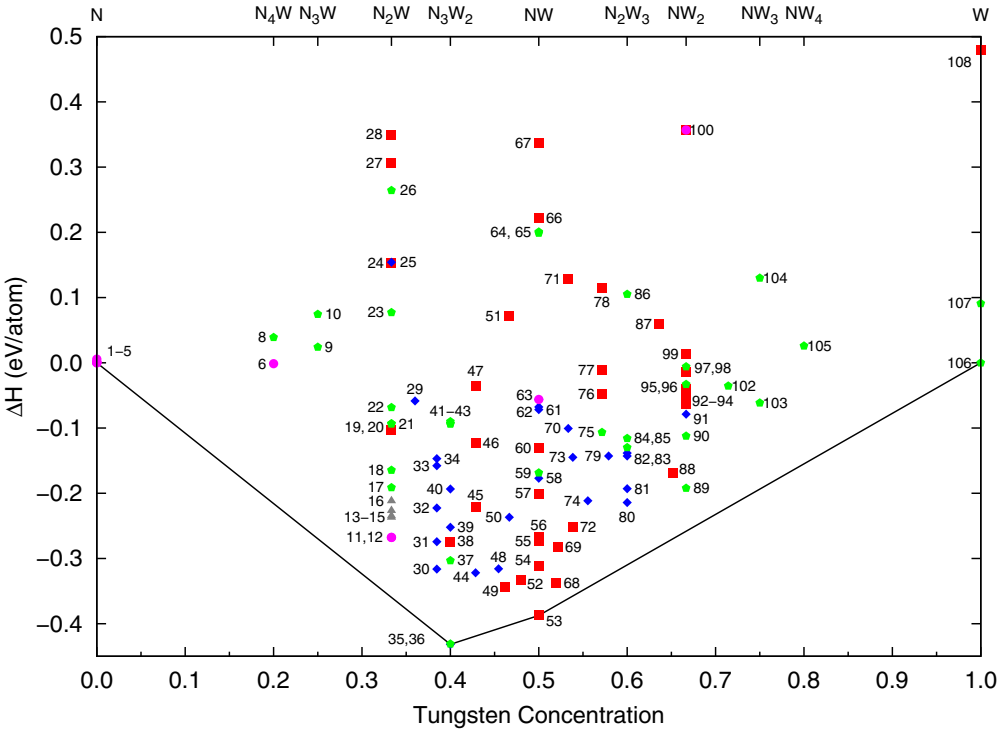

FIG. 2. (Color online) The relative enthalpy (1) of $N_{1-x}W_x$ for the 108 structures listed in the Supplemental Material [48] plotted versus increasing tungsten concentration. These points were calculated using the Perdew-Burke-Ernzerhof (PBE) functional with VASP. Note that the enthalpy of structure #7 is above the upper limit of the graph. The meaning of the symbols is described in the caption to Fig. 1.

the face-centered-cubic structure (#108). Table II shows the equilibrium lattice constants for tungsten as a function of structure and density functional, as well as the energy difference predicted between the ground-state bcc structure and the other two structures. As usual, LDA underestimates the equilibrium lattice constant, while PBE overestimates it, and

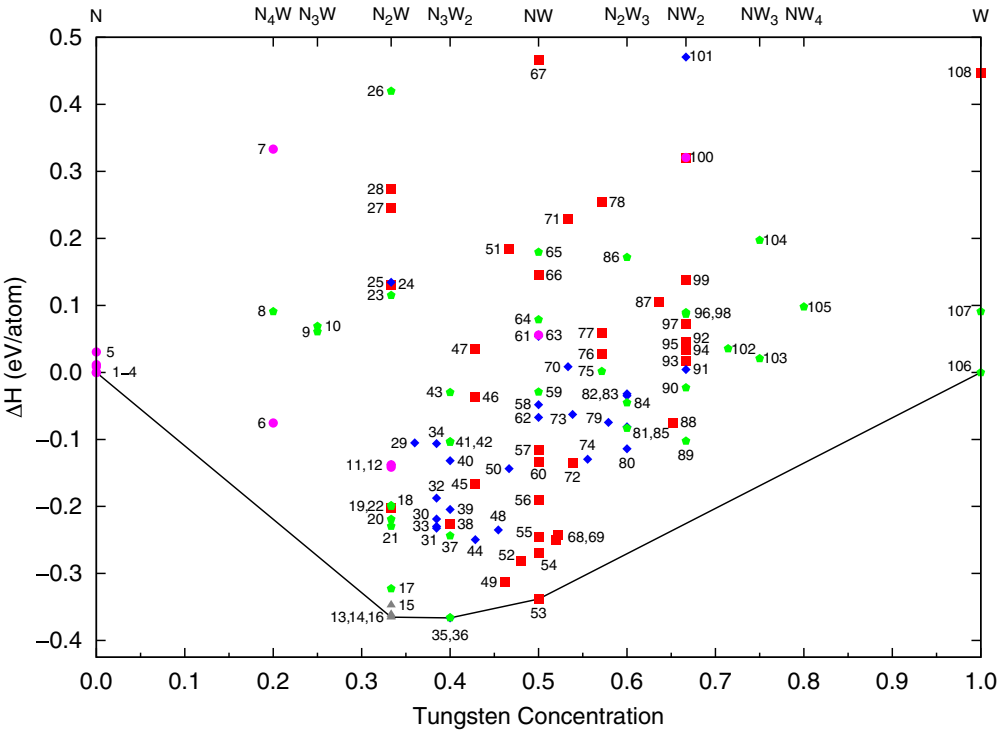

FIG. 3. (Color online) The relative enthalpy (1) of $N_{1-x}W_x$ for the 108 structures listed in the Supplemental Material [48] plotted versus increasing tungsten concentration. These points were calculated using the van der Waals vdW–DF2 functional with VASP. The meaning of the symbols is described in the caption to Fig. 1.

TABLE I. Equilibrium lattice constant, internal parameter, and equilibrium bulk modulus for the $Pa\bar{3}$ structure (#1) of αN_2, as determined using various density functionals and compared to experiment [45,85]. The lattice is simple cubic, and the nitrogen atoms sit on the (8*c*) Wyckoff position, which has one internal parameter x. The equilibrium lattice constant and bulk modulus are determined from a fourth-order Birch fit. The quantity d(N-N) is the length of the nitrogen-nitrogen bond in N_2 molecules.

Functional	LDA	PBE	vdW–DF2	Expt. [45]
a (Å)	5.223	6.187	5.511	5.659
x	0.061	0.052	0.058	0.056
d(N-N) (Å)	1.10	1.11	1.11	1.10
K_0 (GPa)	5.70	0.788	4.69	1.2 [85]

the vdW–DF2 lattice constant is even larger. All functionals give approximately the same energy difference between the three structures, indicating that the van der Waals contribution to the energy is, as one would expect, negligible for pure tungsten.

B. β-phase structures

The β-phase structures [14] (including the γ-NW phase described by Kiessling and co-workers [17–19]) can be described as tungsten nitride in the NaCl structure with vacancies on selected nitrogen and/or tungsten sites. In the extreme limits, this leads to the NaCl structure (#67 in the Supplemental Material [48]), with no vacancies, and a face-centered-cubic structure of tungsten (#108), with all nitrogen sites empty. Experiments [14–19,21,23] generally assume that the tungsten sites in β (and γ) N-W are fully occupied, and that changes in stoichiometry are controlled by vacancies on the nitrogen sites, with possible tetrahedral nitrogen interstitials for the nitrogen-rich phases. As we will see in the following, density functional calculations do not support this point of view.

The lowest-energy β-phase structure, independent of the choice of functional, is NbO (#53) [68], a simple cubic supercell of NaCl with vacancies at the corners and in the center of the cube, as shown in Fig. 4. In itself this should not be particularly surprising, as NW and NbO have the same number of electrons in the valence band. However, no experimental papers claim discovery of the NbO structure. The closest structure to NbO was described by Kiessling and Peterson [16] as a structure with space group $Pm\bar{3}m$ with metal atoms

TABLE II. Equilibrium lattice constants in Å and relative energy differences in eV/atom for the body-centered-cubic (#106), A15 (#107), and face-centered-cubic structures (#108), compared to experimental information where available [41].

	bcc		A15		fcc	
Functional	a	ΔH	a	ΔH	a	ΔH
LDA	3.1426	0.000	5.0151	0.098	3.9814	0.489
PBE	3.1893	0.000	5.0892	0.091	4.0431	0.480
vdW–DF2	3.2503	0.000	5.1850	0.091	4.1211	0.447
Expt.	3.1651		5.048			

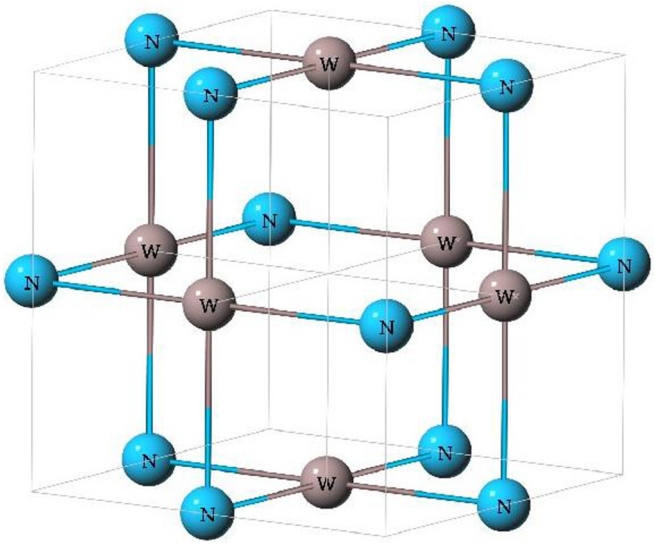

FIG. 4. (Color online) Tungsten nitride in the NbO structure [68] (#53 in the Supplemental Material [48]) constructed by taking equally spaced vacancies from both sites of the NaCl structure. The PBE functional predicts the equilibrium lattice constant to be 4.131 Å.

on the (3*c*) Wyckoff sites. Instead of nitrogen occupying the (3*d*) Wyckoff sites, as would be found in NbO, they found both oxygen and nitrogen on the (1*b*)[1/2 1/2 1/2] and (3*d*) sites, equivalent to the S_3U_4 structure [65]. WYL+ [21] described a structure which they call "c-W_3N_4" ($x = 0.429$) containing no oxygen, which also takes on the S_3U_4 structure. While we did examine this structure (#47), we did not find it particularly close to the ground-state hull using any functional, although it does have a lower value of ΔH than the NaCl structure.

The NbO structure for tungsten nitride was recently examined by Liu, Zhou, Gall, and Khare [67], who computed its equilibrium lattice constants and elastic constants. They did not, however, compare its stability to the NaCl structure, nor find its place in the overall tungsten nitride phase diagram.

Our results show that many low-energy β-type structures in the N-W system can be constructed starting with supercells of the NaCl structure and removing selected N and W atoms. The general rule we found is that the resulting structure will have lower energy than NaCl if the resulting vacancies are not nearest neighbors (separation $a/\sqrt{2}$ for like atoms, $a/2$ for unlike atoms). This includes structures with large atomic relaxations, e.g., the Mo_2N structures [90] (#19 and #92), and structures which only allow relaxation of the lattice constant, e.g., S_3U_4 (#47 or #78) and the ground-state NbO structure.

The elastic constants of the NbO phase are given in Table III, along with the results of Liu *et al.* [67]. Each functional predicts this structure to be quite stiff, with bulk moduli about 30% smaller than diamond while the shear modulus is about 60% of diamond. This is somewhat stiffer than the moduli predicted by Aydin *et al.* [30] for their ReP_4 structure, and nearly as stiff as the N_2W structures predicted by Wang *et al.* [26]. While this is no guarantee that the structure is in fact hard, it does indicate that the NbO structure of tungsten nitride is a candidate for a superhard material. Unlike the N_2W and N_4W candidate structures mentioned elsewhere, every

TABLE III. Equilibrium lattice and elastic constants of tungsten nitride in the NbO structure [space group $Pm\bar{3}m$ #221, Wyckoff positions (3*c*) and (3*d*), #53 in the Supplemental Material [48]]. These were computed by VASP using the appropriate PAW potentials for each exchange-correlation functional. Elastic constants (in GPa) were computed by finite strain [80,81]. The isotropic shear modulus *G* is the average of the Hashin-Shtrikman bounds for a cubic system [88,89]. Starred results are from the paper of Liu, Zhou, Gall, and Khare [67].

Functional	a (Å)	C_{11}	C_{12}	C_{44}	B	G
LDA	4.078	884	140	177	388	239
PBE	4.131	754	126	173	335	220
vdW–DF2	4.208	655	120	154	298	192
LDA*	4.063	903	131	174	388	240
PBE*	4.120	813	115	171	348	227

functional predicts the NbO structure to be the ground-state structure at this composition.

In addition to the elastic constants shown in Table III, we further checked the stability of the NbO structure by computing the phonon spectra, as shown in Fig. 5. There are no imaginary frequency modes, indicating that the structure is stable.

The electronic band structure and density of states of the NbO phase are shown in Figs. 6 and 7, respectively. As in all cases in this paper, the high-symmetry k points are labeled following as in Lax [91] and by AFLOW [92]. The structure is a metal, with most of the electrons at the Fermi level being provided by the tungsten d states.

The change in enthalpy ΔH for each of our β-phase structures is shown in Fig. 8. This is a subset of Fig. 2 containing only β-phase structures. Each point is color coded to show the concentration of vacancy sites on the underlying NaCl lattice, e.g., the NbO structure (#53) is a supercell of

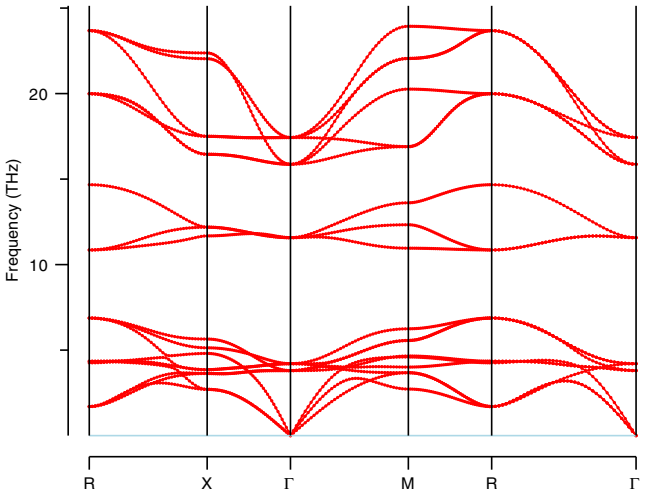

FIG. 5. (Color online) Phonon frequencies along high-symmetry lines for the NbO structure (#53) of tungsten nitride, found with the MedeA® package [79]. No imaginary phonon frequencies were found, indicating that this structure is stable against small amplitude vibrations. The high-symmetry points and lines are described in the Supplemental Material [48].

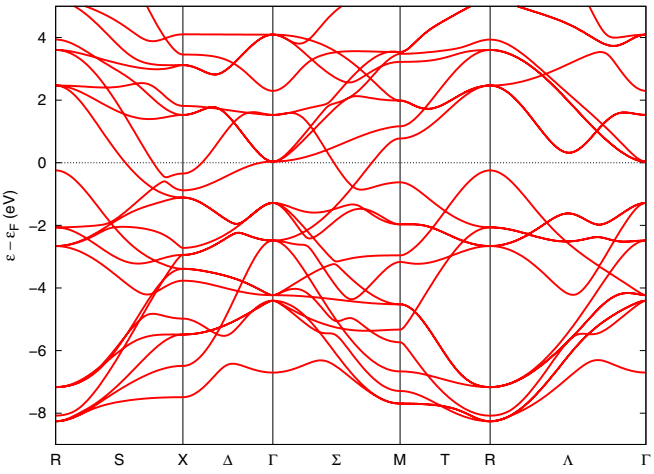

FIG. 6. (Color online) The electronic band structure of tungsten nitride in the NbO structure (#53) at the PBE equilibrium (a = 4.131 Å). The high-symmetry points and lines are described in the Supplemental Material [48].

the NaCl structure with 25% of its sites vacant. We see that the lower-energy structures, particularly in the region of 50% tungsten, are dominated by unit cells with 25% or fewer vacancies. This suggests that the experimentally observed β-NW structures have the atoms arranged in a sodium chloride structure where each site is approximately 75% occupied, the exact vacancy fraction for each site depending on the composition. This picture fits with the experimental lattice constant [22] for the the β phase, which at 4.12–4.14 Å is similar to the lattice constants we obtain for the NbO structure (4.08 Å LDA, 4.13 Å PBE), and far below the lattice constant we obtain for the fully occupied NaCl structure (4.30 and 4.37 Å, respectively).

Contrary to published results [14–16,18,19,23], we see no evidence of stable β-phase NW_2 structures, nor of any structures where all of the tungsten sites are occupied. For x

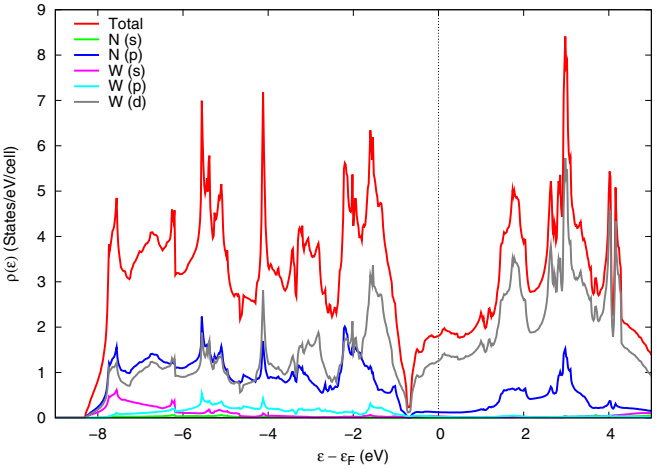

FIG. 7. (Color online) The electronic density of states and angular momentum decomposed density of states for tungsten nitride in the NbO structure (#53). These were computed via the tetrahedron method in VASP. The primary contributions are from the N-p and W-d states, with the W-d states dominating the conduction band.

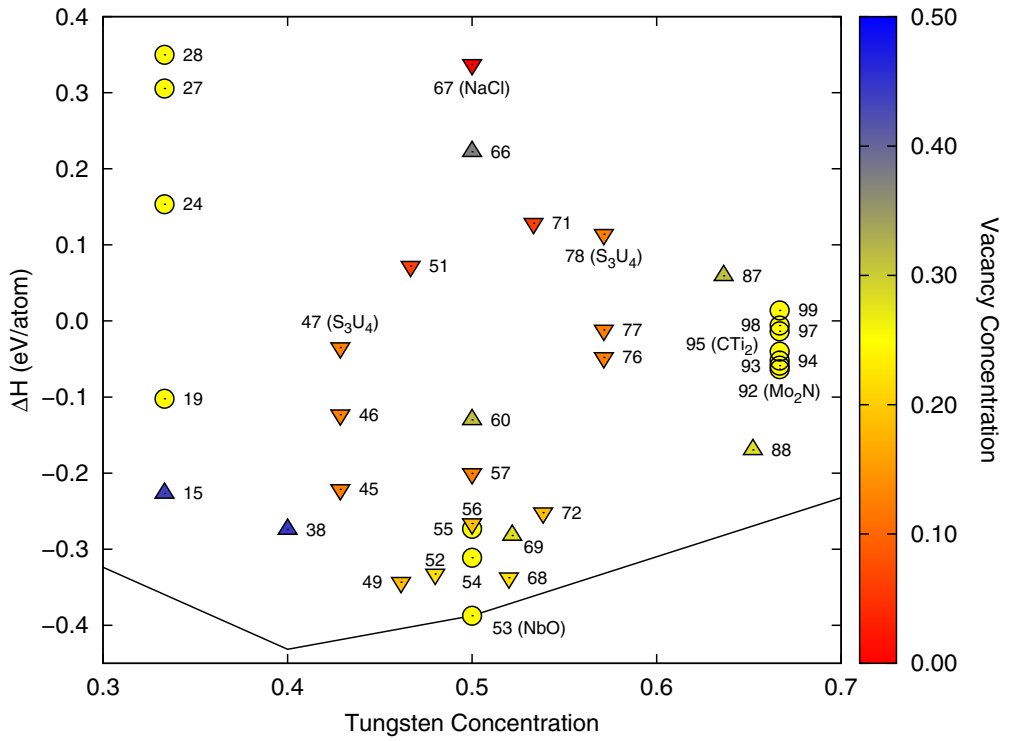

FIG. 8. (Color online) A section of Fig. 2 showing only structures created by removing atoms from supercells of the NaCl structure. Yellow circles denote structures where 25% of the sites on the NaCl lattice are empty. Downward-pointing triangles have fewer than 25% of the sites vacant, and the redder triangles have fewer vacancies, culminating in the NaCl structure (#67). Upward-pointing triangles have more than 25% of the sites vacant, and are bluer as more sites become vacant. Known experimental structures are labeled by their prototype name.

near $\frac{2}{3}$, the closest structure β-phase structure to the tie line is a N_8W_{15} structure (#88), which has a vacancy on the tungsten site as well as multiple vacancies on the nitrogen sites of the NaCl supercell. This suggests that vacancies on both nitrogen and tungsten sites are important in stabilizing any cubic (β) tungsten nitride structure.

C. δ-phase structures

While the β (and γ) phases in the N-W system can all be described by various patterns of both nitrogen and tungsten vacancies in supercells of the sodium chloride structure, δ phases consist of alternating triangular sheets of nitrogen and tungsten atoms, stacked in hexagonal or rhombohedral patterns, as in tungsten carbide and nickel arsenide, with experiments [18,19,21] suggesting that vacancies appear only on the tungsten sublattices.

Schönberg [49] suggested that the parent δ phase is the tungsten carbide structure (#61 in the Supplemental Material [48]), with vacancies on the nitrogen sites. He did not pursue this idea, as at the time the determination of nitrogen positions in a tungsten nitride compound was impossible.

The first large-scale investigation of δ phases was done by Khitrova and Pinsker [18]. They found six δ-phase structures, ranging in composition from N_2W (δ_R^V, structure #25 in the Supplemental Material [48]) to NW_2 (δ_H^{II}, #101). While these end points do not have any vacancies, the intermediate structures ($\delta_H^{I,III,IV}$, δ_R^{VI}) have vacancies on some tungsten planes.

Recently, WYL+ [21] found experimental evidence for a δ-type rhombohedral structure which they designated "r-W_2N_3" ($x = 0.4$). This structure consists of close-packed planes of alternating layers of tungsten and nitrogen, with the stacking pattern ABABCACABCBC. Alternating planes of tungsten have an occupation factor of $\frac{1}{3}$, i.e., two-thirds of the tungsten sites are vacant, giving the N_3W_2 stoichiometry. Interestingly, WYL+ also considered a structure which they called "h-W_2N_3" ($x = 0.6$, #80); this structure is identical to the parent (i.e., no tungsten vacancies) δ_H^I structure of Khitrova and Pinsker (#80), except that placement of the tungsten and nitrogen atoms is reversed.

As we saw with the β-phase structures, atomistic calculations cannot readily model randomly placed vacancies. We approximated the random structures by creating supercells of the parent structures, and then removing various patterns of tungsten atoms to match the required stoichiometry. We also looked at structures slightly off the target stoichiometry. The Supplemental Material [48] describes the low-lying (within 0.2–0.3 meV/atom of the convex hull) structures we found by this method. It is necessarily incomplete, but we believe we have found structures extremely close to the actual minimum-energy structures.

Figure 9 shows some of the low-energy structures in this system, as a function of tungsten concentration (along the x axis) and vacancy concentration (shading). We started by fully occupying all the tungsten sites in the six δ phases described by Khitrova and Pinsker [18,19], the "r-W_2N_3" phase found by WYL+ [21] (the circled structures in the diagram), and the WC structure (pentagons) proposed by Schönberg [49]. We then systematically removed atoms from the appropriate tungsten layers. In most cases, this lowered ΔH, and two

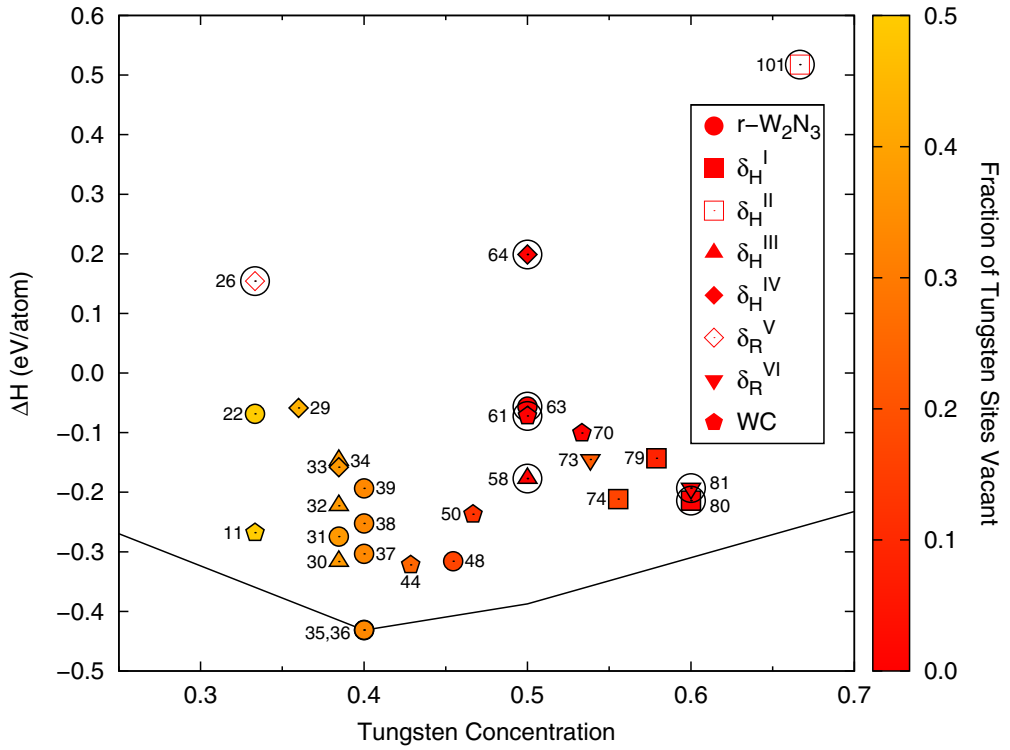

FIG. 9. (Color online) Enthalpy per atom for various crystal structures approximating the δ phases of Khitrova and Pinkser [18,19] and Wang, Yu, Lin *et al.* (WYL+) [21]. All calculations were done using the PBE functional. The legend describes the six structures found by Khitrova and Pinsker, as well as the "r-W_2N_3" structure of WYL+. We also include the tungsten carbide (WC) structure and some derivatives [25,49]. The actual structures are labeled according to the indexing in the Supplemental Material [48]. The circled structures are the parent structures, which have fully occupied tungsten sites. For the other structures, the tungsten vacancy concentration is indicated by the point shading. Red (dark) shaded structures have no or few defects, while orange-yellow (light) shading indicates a larger concentration of vacancies, up to 50%. Note that some tungsten planes have no vacancies, while other planes can have as many as $\frac{2}{3}$ of the sites vacant. See Fig. 10 for an example. The δ_H^I and δ_H^V structures have no vacancy sites, therefore, the parent is the only structure we studied and its special status is shown by having no coloring to the data point.

of our derivative "r-W_2N_3" structures (#35 and #36) have the lowest ΔH of all structures in this study, independent of choice of functional. In addition, the two structures (which are numerically degenerate in energy) form part of the convex hull for the N-W system. The "h-W_2N_3" phase mentioned above is approximately 0.35 eV/atom above the ground-state phase, so it is at best a metastable state.

Of the two ground-state structures, #35 has a smaller unit cell than #36, so we will concentrate on it. Figure 10 shows the atomic positions for this structure. Its elastic constants, listed in Table IV, were computed using the finite displacement method contained in VASP, and were used to calculate the Reuss (lower) and Voigt (upper) bounds on the isotropic polycrystalline bulk and shear moduli [55]. The shear modulus is less than 200 GPa, so we cannot regard this as a candidate for a superhard structure.

The electronic band structure is shown in Fig. 11, and the electronic density of states in Fig. 12. There is a small density of states at the Fermi level, so this structure is a semimetal. We only show the results for the PBE calculation, but this behavior persists across all three choices of DFT. Similar behavior occurs in the nearly degenerate structure #36.

Another low-energy δ-type structure is the $hP3$ N_2W structure proposed by WLLX+ [26], which can be constructed by doubling the tungsten carbide (#61) unit cell in the z direction and removing one of the tungsten atoms. This structure is composed of N_2 dimers alternating with layers of tungsten, and so we will discuss it in the next section, although we do include it in Fig. 9.

In addition to the structures described above, we also looked at the structure labeled "h-W_2N_3" by WYL+ [21], which is same as the δ_H^I N_2W_3 structure #80 with N and W occupations reversed, forming structure #43. The αSm structure [93], structures #25 and #91, consists of alternating close-packed layers (stacking NNW or NWW), and so can also be considered a δ phase. Finally, we tried modeling δ-like structures starting with N-W in the NaCl structure, considering it as a close-packed system with stacking ABCABCABC, removing two-thirds of the atoms in alternating tungsten layers, forming structure #38. While these structures had $\Delta H < 0$, they were not near the convex hull using any functional.

D. N_2 phases

For our purposes, an N_2 phase is one in which we can readily identify nitrogen dimers inside a tungsten matrix. Aydin, Ciftci, and Tatar (ACT) [30] studied N_4W in the ReP_4 structure [63] (Supplemental Material structure #7) They equilibrated the system using the LDA functional and found a negative value for ΔH, and also computed the elastic constants and an

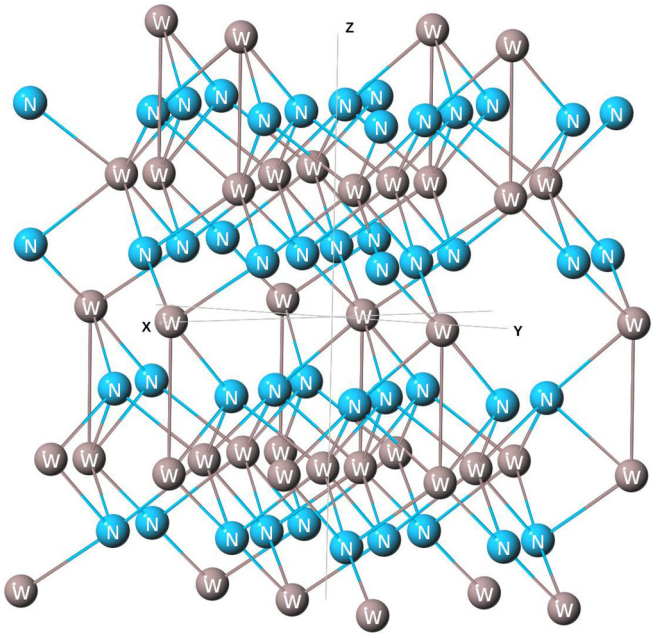

FIG. 10. (Color online) The PBE minimum-energy structure #35, space group $Cm - C_x^3$ (#8). This is an approximation to the "r-W_2N_3" structure, and has the proper number of tungsten vacancies in the unit cell [21]. In the experimental "r-W_2N_3" structure, the tungsten sites in the $z = 0$ plane are randomly occupied and do not necessarily have the pattern shown here.

estimate of the hardness, stating that this material should be superhard.

In the form proposed by ACT, this structure is of type N_2, with elongated nitrogen dimers in a tungsten matrix. It is extremely difficult to equilibrate. Starting from the structure which the authors graciously provided us, we found a minimum-energy structure (#7) close to theirs as shown in Fig. 1. Unfortunately, we found that $\Delta H > 0$, suggesting a difference in end-point energies in Eq. (1) in our calculation compared to ACT. In addition, when we used the ACT structure

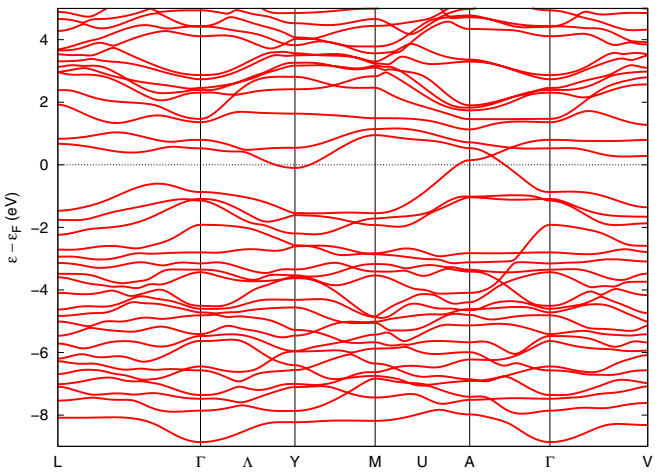

FIG. 11. (Color online) The electronic band structure for structure #35, one of our approximations to the "r-W_2N_3" structure [21], using the PBE functional.

TABLE IV. Density functional dependent elastic constants of structure #35, space group Cm(#8), Pearson symbol $mC20$, shown in Fig. 10. This is an approximate version of the "r-W_2N_3" structure [21]. We also include the Reuss (lower) and Voigt (upper) bounds on the isotropic polycrystalline bulk and shear moduli for these systems [55]. All distances are in Å, while the moduli are in GPa. Unlisted elastic constants are zero by symmetry. Note that the Reuss bulk modulus B_R is the equilibrium bulk modulus of the crystal given by $K_0 = -V_0 P'(V_0)$, where V_0 is the equilibrium volume of the crystal.

Functional	LDA	PBE	vdW–DF2
Lattice parameters			
a (Å)	4.963	5.035	5.132
b (Å)	8.547	8.666	8.836
c (Å)	6.015	6.101	6.213
β (°)	56.732	56.784	56.823
Elastic constants (GPa)			
C_{11}	611	555	484
C_{22}	637	577	501
C_{33}	521	482	428
C_{44}	171	153	130
C_{55}	185	165	142
C_{66}	201	185	161
C_{12}	184	162	139
C_{13}	165	143	120
C_{23}	143	122	101
C_{15}	15	11	6
C_{25}	−6	−3	2
C_{35}	5	4	5
C_{46}	−10	−6	−1
Bulk modulus (GPa)			
Reuss (B_R)	303	272	235
Voigt (B_V)	306	274	237
Shear modulus (GPa)			
Reuss (G_R)	194	177	117
Voigt (G_V)	197	180	137

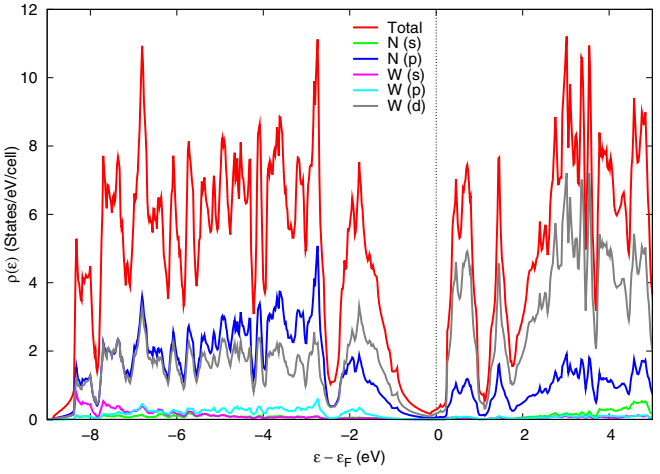

FIG. 12. (Color online) The electronic density of states for structure #35, one of our approximations to the "r-W_2N_3" structure [21], using the PBE functional and the tetrahedron method. Note that the angular momentum decomposed densities of states are summed over all atoms of the same type, even if they have different crystallographic positions.

with the PBE and vdW–DF2 functionals, we found ΔH to be large and positive, over 0.7 eV/atom in the PBE case.

Furthermore, with some manipulation of the structures we were able to obtain even lower-energy structures (#6). In the LDA case, we swapped the positions of the tungsten atoms with the second set of nitrogen atoms, and found an $\Delta H < 0$ and much closer to the convex hull, though still not on it. This procedure did not lead to a low-energy structure for the PBE or vdW–DF2 functions, but when we expanded the volume of the LDA structure we found a double-well structure in the energy, where the higher volume had a lower energy. Backtracking from this, we found an even lower-energy structure at a volume comparable to the original LDA/ACT structure. When we used this minimized structure with the PBE and vdW–DF2 functionals, we obtained the structures designated (#6) in the Supplemental Material [48].

Given these results, we must conclude that the ACT structure is not the lowest-energy structure related to ReP_4, that is, with space group $Pbca$ and all atoms on ($8c$) Wyckoff sites. In addition, all of the ReP_4 structures are least 0.1 eV above the convex hull of the WN system, and so unlikely to be seen. However, we are not certain that we have found the minimum-energy structure within these constraints, for any choice of density functional, and we are continuing the search.

In addition to the ReP_4 structure, we looked other candidates for the N_4W ground state. The only low-energy structure we found was related to the metastable FeB_4 structure proposed by Van der Geest and Kolmogorov [70]. We originally found the enthalpy of this structure to have $\Delta H \approx 1$ eV using the PBE functional. On transferring this structure from one computer to another we inadvertently transposed some atomic positions. The resulting structure, #8, is much lower in energy than the original converged structure, independent of the choice of functional, but it is still far from the convex hull.

Given that we have found two structures with relatively low enthalpies, we cannot eliminate the possibility that a stable N_4W compound exists, but at the moment this seems unlikely.

Compounds with stoichiometry N_2W have been studied by other workers. WLLX+ [26] used an evolutionary method and found two nearly degenerate structures which we designate as #11 and #12. These are N_2 dimers stacked in a hexagonal crystal alternating with tungsten atoms. The structures differ by the stacking patterns of the dimers, and they could be classified as either N_2 phases or as δ phases with missing tungsten planes.

Table V gives the equilibrium lattice constants and elastic constants of the two structures using all three density functionals. We compare our results to those of WLLX+, who looked at the systems using LDA and PBE. In all cases, both structures have relatively large bulk and shear moduli, and so are candidate superhard materials.

The structures #11 and #12 are the lowest-energy N_2W systems within our LDA and PBE calculations. In the LDA they form part of the convex hull for the tungsten nitrogen system, as shown in Fig. 1.

TABLE V. Equilibrium structural parameters for the hexagonal N_2W structures found by Wang *et al.* (hereafter WLLX+) [26]. The low-symmetry $hP3$ structure (#11 in the Supplemental Material [48]) is in space group $P\bar{6}m2$, with nitrogen atoms at the ($2g$) Wyckoff positions ($00z$) and the tungsten atom on the ($1d$) site ($\frac{1}{3}\frac{2}{3}\frac{1}{2}$). In the high-symmetry $hP6$ structure (#12, $P6_3/mmc$), the nitrogen atoms are on ($4e$) sites ($00z$), and the tungsten atoms are on ($2d$) sites ($\frac{1}{3}\frac{2}{3}\frac{3}{4}$). For the LDA and PBE functionals, we show our results (O), along with the results of WLLX+. $R_{N\text{-}N}$ and $R_{N\text{-}W}$ are the length of the respective bonds. The elastic constants are in GPa. The isotropic bulk (B) and shear (G) moduli are averages of the Reuss and Voigt bounds [55].

	LDA		PBE		
	Low-symmetry		$P\bar{6}m2$, $hP3$		vdW–DF2
Functional	O	W	O	W	O
a (Å)	2.887	2.887	2.928	2.933	3.000
c (Å)	3.877	3.877	3.916	3.918	3.974
z	0.1804	0.1804	0.1813	0.1814	0.1824
$R_{N\text{-}N}$ (Å)	1.399	1.399	1.421	1.421	1.450
$R_{N\text{-}W}$ (Å)	2.077	2.077	2.104	2.104	2.143
C_{11}	638	654	573	588	493
C_{33}	1056	1082	954	973	827
C_{44}	241	260	222	232	191
C_{12}	207	213	183	191	159
C_{13}	230	248	193	206	157
B	396	412	351	255	297
G	246	255	226	231	195
	High-symmetry $P6_3/mmc$, $hP6$				
	O	W	O	W	O
a (Å)	2.893	2.893	2.939	2.939	3.007
c (Å)	7.714	7.714	7.796	7.796	7.891
z	0.0898	0.0898	0.0902	0.0902	0.0907
$R_{N\text{-}N}$ (Å)	1.392	1.392	1.406	1.406	1.431
$R_{N\text{-}W}$ (Å)	2.078	2.078	2.105	2.105	2.144
C_{11}	633	642	568	579	486
C_{33}	1051	1078	952	973	827
C_{44}	249	262	228	233	197
C_{12}	213	217	187	195	161
C_{13}	237	252	199	211	197
B	399	411	353	364	298
G	245	252	225	228	195

E. SiO_2 phases

One of our approximate β-phase constructs, which we will designate $cI36$ (#15 in the Supplemental Material [48]), had a surprisingly low enthalpy when we calculated its energy using the van der Waals vdW–DF2 functional. The $cI36$ structure starts from a 32-atom body-centered-cubic supercell of the NaCl structure, with 4 nitrogen atoms and 10 tungsten atoms removed. This leaves only the ($24h$) and ($12d$) Wyckoff positions occupied, and so we originally classified it as a β-phase structure. However, as seen in Fig. 13 and described in Table VI, each tungsten atom is bonded to four nitrogen atoms arranged tetrahedrally, and each nitrogen atom is bound to two tungsten atoms. This arrangement is reminiscent of many SiO_2 structures [69], although this particular structure has not been seen experimentally.

We also looked some of the simpler SiO_2 structures, including the high-temperature phase of quartz [94] (#16 in the Supplemental Material [48]), cristobalite [95] (#14), and tridymite [96] (#13). The low-temperature forms of these

TABLE VI. The $cI36$ structure of N_2W, constructed from a 32-atom body-centered-cubic supercell of the NaCl structure. The space group is $Im\bar{3}m$-O_h^9 (#229), the nitrogen atoms occupy the ($24h$) Wyckoff positions ($0yy$), and the tungsten atoms occupy the ($12d$) sites ($0\frac{1}{4}\frac{1}{2}$). The first N-W-N angle is for atoms lying on the surface of the cube cell. The second case has one of the N atoms in the interior of the cube.

Functional	LDA	PBE	vdW
a (Å)	10.273	10.383	10.490
y	0.1454	0.1455	0.1455
N-W bond (Å)	1.840	1.860	1.879
	Angles		
W-N-W	108.7°	108.6°	108.5°
N-W-N (face)	108.7°	108.6°	108.5°
N-W-N (interior)	109.9°	109.9°	110.0°

structures are degenerate with these, so we do not report them here. At $x = \frac{1}{3}$ the high-temperature quartz structure had the lowest enthalpy when using the van der Waals–DF2 functional, and it forms part of the ground-state hull in Fig. 3.

We also looked at some distorted rutilelike structures, which have bonding similar to SiO_2. These include bixbyite [97,98], structures #41 and #42; βNbO_2 [99], structure #17; and PbO_2 [100] structure #21, which has the same valence electron count at NbO_2. These structures had energies comparable to the SiO_2 structures discussed above. In particular, the relaxed βNbO_2 structure is quite close to the convex hull when we used the vdW–DF2 functional.

All of the these structures are insulating. Since the cubic $cI36$ structure was the first of these we found, and has the highest-symmetry primitive cell, we did band-structure calculations for it, as shown in Fig. 14. There is a direct band gap of 0.75 eV using the vdW–DF2 functional. The band structure is unusual in that there is a very flat band (0.05 eV maximum dispersion) at the top of the valence band. As shown in the electronic density of states plot, Fig. 15, this narrow band has strong nitrogen $2p$ character.

We also computed the elastic constants for the $cI36$ structure. Not surprisingly, this very low-density system has small elastic constants, as shown in Table VII. We expect the other SiO_2 structures to have similar shear moduli.

Given the large density of states near the top of the occupied bands in this system, we looked for structural

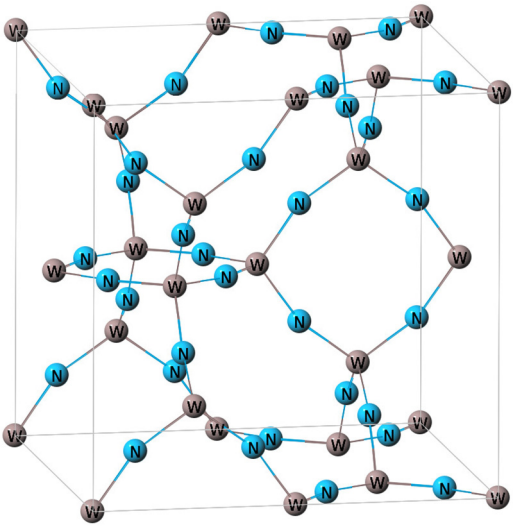

FIG. 13. (Color online) The SiO_2-like $cI36$ structure (#15 in the Supplemental Material [48]) predicted as the ground state of N_2W by the vdW–DF2 functional. The basic structure looks the same using LDA, PBE, and vdW–DF2 functionals. The exact dimensions are described in Table VI. Note that this is a body-centered-cubic lattice, so the center of the cube and the cube corners are equivalent sites. The inversion sites are at the centers of the eight-atom rings, not on the tungsten atoms.

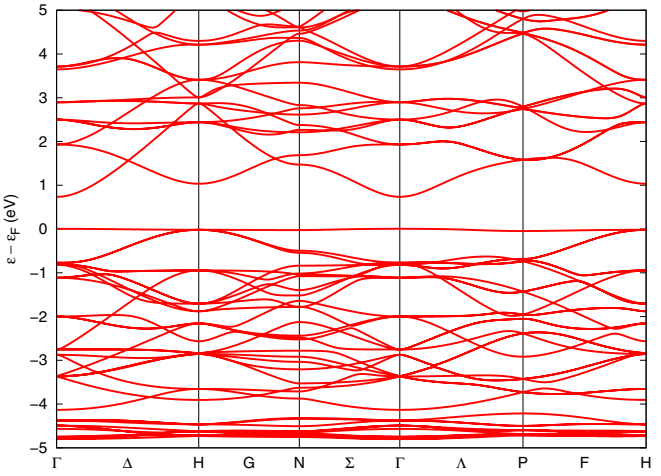

FIG. 14. (Color online) The electronic band structure for the SiO_2-like body-centered-cubic $cI36$ structure (#15) of N_2W described in the text. Calculations were done using the vdW–DF2 functional, including van der Waals forces, within VASP. The top valence band has a very small dispersion, dropping to −0.05 eV below the top of the valence band at P. The gap is 0.75 eV, and is direct at Γ. The LDA and PBE calculations produce similar band structures.

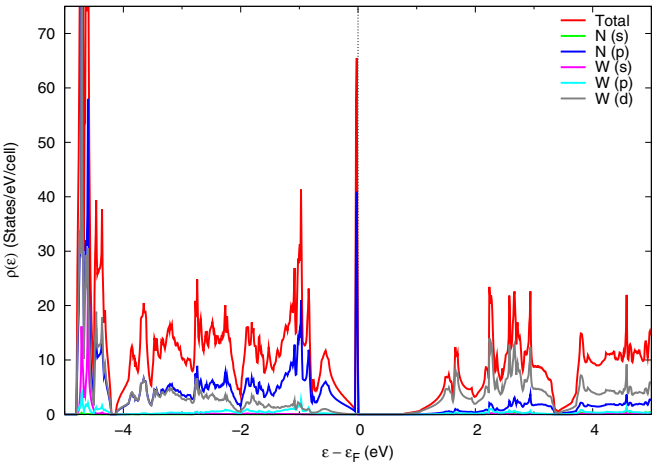

FIG. 15. (Color online) The electronic total, and angular momentum decomposed, density of states for N_2W in the SiO_2-like $cI36$ structure (#15), using the vdW–DF2 functional and the tetrahedron method within VASP. We truncated the plot at 75 states/eV/cell in order to show the behavior of the system near the top of the valence band. The density of states at the bottom of the valence band approaches 200 states/eV/cell.

TABLE VII. Elastic constants for the $cI36$ structure of N_2W, computed using the LDA, PBE, and vdW–DF2 functionals. Elastic constants were computed by the finite strain method [80], allowing the atoms to relax at each strain while fixing the unit cell. Equilibrium structural parameters are taken from Table VI. B is the equilibrium bulk modulus, and all elastic constants are in GPa. The shear modulus G is an average of the Hashin-Shtrikman bounds [88,89].

Functional	C_{11}	C_{12}	C_{44}	B	$C_{11}-C_{12}$	G
LDA	119	77	13	91	42	15
PBE	112	72	13	85	41	16
vdW–DF2	104	65	12	78	39	14

instabilities, including imaginary phonon frequencies and a possible magnetic state. While we have not done a complete examination of the phonon spectrum, those k points we sampled all have positive phonon frequencies, and imposing a spin polarization on the crystal raises its energy. We conclude that the structure is at least metastable.

While all of SiO_2 structures we examined always have $\Delta H < 0$, none of them form part of the convex hull when we use the PBE or LDA functionals. The appearance of these structures on and near the vdW–DF2 convex hull (Fig. 3) is most likely an artifact of the van der Waals density functional.

F. Miscellaneous structures

In this section, we describe several low-energy structures that appear in Figs. 1–3. Many of these structures have been studied by others, as outlined in Sec. II.

While we did calculations for a number of structures with composition NW_2, including β and δ phases, the most interesting structures we found were NW_2 in the hexagonal MoS_2 structure [101] (#89) and the rhombohedral αMoS_2 structure [102] (#90). In all cases, the hexagonal MoS_2 structure had the lowest enthalpy of any NW_2 structure we studied, and within the LDA it was nearly touching the tie line. This structure has not been seen nor previously predicted in the N-W system. We show the LDA equilibrium structure in Fig. 16. While exhibiting the layered character of the MoS_2 structures, it is not two dimensional. In fact, the distance between atoms in adjacent tungsten layers (2.81 Å) is smaller than the distance between tungsten atoms in the plane (2.84 Å).

This structure was only run because it was available in the AFLOW database. If it had not been present there, it would not have been tested since we had no indication either experimentally or theoretically that the N-W system would support close-packed tungsten planes. This demonstrates the power of the structural database in investigating new systems.

Since this structure has a similar form to the δ structures, we tried to lower its energy by placing vacancies on the tungsten sites (#85 in the Supplemental Material [48] tables and in Figs. 1–3) and by adding interplaner nitrogen or tungsten atoms (#75, #89). In no case were we able to get an enthalpy below the parent MoS_2 structure.

This structure is close to the convex hull in the LDA, and in the hopes of finding an instability leading to a lower-energy structure, we did a preliminary test for hardness by computing the elastic constants of the hexagonal MoS_2 phase, shown in Table VIII. It is not particularly hard, having a shear modulus on the order of 100 GPa. It is, however, elastically stable, as the elastic constants satisfy the Born criterion [39]. The structure is metallic, as can be seen from the band structure (Fig. 17) and electronic density of states (Fig. 18) .

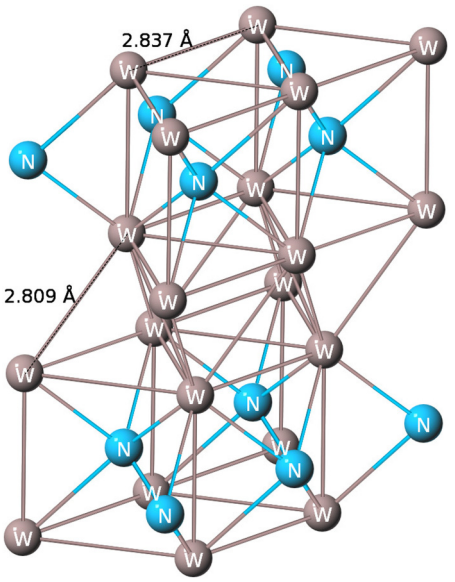

FIG. 16. (Color online) NW_2 in the hexagonal MoS_2 structure [101] #89 in the Supplemental Material [48]. Unlike MoS_2, the interplaner W-W distance is smaller than the in-plane W-W distance.

We looked at various structures with composition NW, including nickel arsenide (#59), studied by Kroll, Schröter,

TABLE VIII. Density functional dependent elastic constants of structure of NW_2 in the hexagonal MoS_2 structure [101] #89 in the Supplemental Material [48]. We also include the Reuss (lower) and Voigt (upper) bounds on the isotropic polycrystalline bulk and shear moduli for these systems [55]. All distances are in Å, while the moduli are in GPa. z is the free coordinate of the tungsten atom at the $(4f)$ Wyckoff site. Since this is a hexagonal crystal, $C_{66} = (C_{11} - C_{12})/2$. Note that the Reuss bulk modulus B_R is the equilibrium bulk modulus of the crystal given by $K_0 = -V_0 P'(V_0)$.

Functional Lattice parameters	LDA	PBE	vdW–DF2
a (Å)	2.837	2.875	2.933
c (Å)	10.212	10.369	10.584
z [W $(4f)$]	0.612	0.612	0.611
Elastic constants (GPa)			
C_{11}	568	512	396
C_{33}	730	668	581
C_{44}	158	142	113
C_{12}	349	312	307
C_{13}	238	207	178
Bulk modulus (GPa)			
Reuss (B_R)	390	349	299
Voigt (B_V)	391	349	300
Shear modulus (GPa)			
Reuss (G_R)	142	130	74
Voigt (G_V)	154	141	102

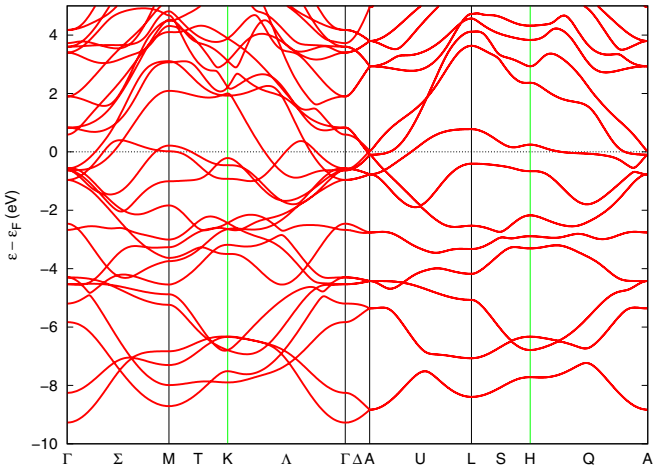

FIG. 17. (Color online) The electronic band structure for NW_2 in the hexagonal MoS_2 structure [101,102] (#89 in the Supplemental Material [48]), using the PBE functional.

and Peters [24], and the zinc-blende structure (#65), studied by WYL+ [21]. The nickel arsenide structure, which could be considered a δ phase, is a few tenths of an eV above the NbO structure. The zinc-blende structure, which WYL+ find to be very stiff, is over 0.5 eV above NbO and so is unlikely to form.

No N_3W structures were found near the convex hull. The closest two were structures molybdite (MO_3 [103], #9) and P_3Tc (#10) [56] Song and Wang [29] studied P_3Tc within the LDA, and found to have reasonable large bulk (303 GPa) and shear (156 GPa) moduli. They also found that it had negative enthalpy (1), which we confirm. However, as shown in Fig. 1, this structure is well above the convex hull within the LDA. The PBE and vdW–DF2 results show that the ΔH for P_3Tc is positive. It is unlikely, therefore, that N_3W exists in the P_3Tc structure.

One-half of the nitrogen atoms in the relaxed molybdite structure (which looks nothing like molybdite) form N_2 dimers with spacing 1.12–1.13 Å. The relaxed P_3Tc structure is similar, with N_2 dimers spaced 1.2 Å apart. We can therefore classify both structures as partial N_2 phases.

Both structures have the same *Pnma* space group, with all atoms occupying (8*c*) Wyckoff positions, so it may be possible to transform from P_3Tc to MoO_3 by simply varying the c/a and b/a ratios. Such a transformation would reveal the structure of the energy barrier between the two states. Since these structures are well above the minimum-energy structure, we have not investigated this further.

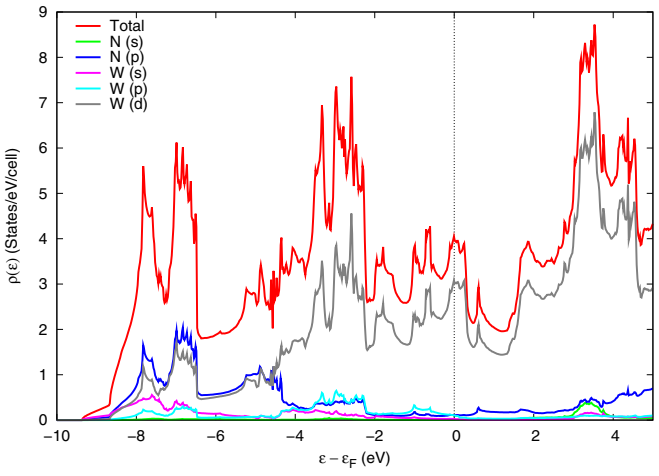

FIG. 18. (Color online) The electronic total, and angular momentum decomposed, density of states for NW_2 in the hexagonal MoS_2 structure [101,102] (#89 in the Supplemental Material [48]), using the PBE functional.

V. DISCUSSION

To truly predict the structure of a compound A_MB_N, we must find the lowest-energy structure at that composition, but we must also determine if that structure is unstable with respect to decomposition into either into its end points or to some intermediate structures. When doing approximate density functional theory calculations, we should also be sure that the predicted structure is stable or metastable with respect to different functionals since current functionals are only approximations to the real one.

Using the tungsten nitride system as an example, the AFLOW high-throughput method was used to calculate the relative enthalpy (1) of over 500 structures at variety of compositions $N_{1-x}W_x$. We then studied over 100 of these structures in detail, using the generalized-gradient PBE functional, the local density approximation, and the van der Waals vdW–DF2 functional to produce a zero-temperature phase diagram over a wide variety of compositions.

For $x \geqslant 0.4$, all three functionals give the same predicted ground states: at $x = 0.4$, a hexagonal δ-NW structure with random vacancies on the tungsten sites, which we approximated using various supercells of the parent structure with different patterns of tungsten vacancies; and the β-NW structure, with the lowest state the ordered NbO structure, the sodium chloride structure with one-fourth of the sites vacant.

All three functionals show the importance of vacancies in the tungsten nitride system. If we consider the sodium chloride and tungsten carbide structures as the parents of the NW β and δ phases, we can nearly always lower the energy by constructing a supercell and removing selected atoms, as shown in Figs. 8 and 9. All of the $0 < x < 1$ structures on the convex hull in Figs. 1–3 can be constructed by removing atoms from supercells of the parent structures. This is in agreement with experiment, which finds random vacancies in almost every structure.

What is not in agreement with experiment is the actual composition of the β phase. We find the lowest-energy structures near $x = \frac{1}{2}$, while experiment tends to favor cubic structures with $x \approx \frac{2}{3}$. The likeliest explanation is in the kinetics of the tungsten-nitrogen reaction. It is very difficult to dissolve N_2 molecules into tungsten [23], and so it is plausible that the energy barriers in the problem will favor tungsten-rich compounds. A thorough investigation of the kinetics of tungsten nitride formation is necessary for further understanding.

As noted, our original motivation for looking at the tungsten nitride system was the possibility of forming hard carbon-free materials. Previous calculations suggested that specific N_2W and N_4W structures were stable, had large bulk and shear

moduli (over 200 GPa), and were candidate hard structures. We found the N_4W compound [30] to be well above the convex hull, so that it would tend to phase separate into N_2 and either N_2W or N_3W_2, depending on the choice of density functional. The candidate N_2W structures [26] are on the LDA convex hull, but not the PBE or vdW–DF2 hulls, and so might be found at some future date. The experimentally observable "r-W_2N_3" structure has the lowest value of ΔH in the entire system. Unfortunately, it is not particularly hard, as our estimated shear modulus is under 200 GPa. However, the β-phase ground-state NbO structure does have shear moduli over 200 GPa, and so might be "hard." This will require more investigation, similar to what Aydin, Ciftci, and Tatar [30] did for their N_4W candidate.

Another surprise coming out of this study is the change in the shape, depth, and composition of the convex hull depending on the choice of density functional. In the absence of spin-polarization effects, the DFT community usually thinks of the generalized-gradient approximation, and especially the PBE and related functionals, as improving on the LDA predictions of lattice constants, but not changing the ordering of structures. For $x \geqslant 0.4$, that is more or less true here. However, for nitrogen-rich systems there is considerable disagreement about the ordering of structures. This is most likely caused by the neglect of van der Waals forces in the nitrogen-rich systems. To test this, we used a common van der Waals functional, vdW–DF2. It indeed provides a better lattice constant for the solid N_2, but it also leads to what seems to be a spurious prediction of the ground-state structure at N_2W. It also consistently overestimates the lattice constants for systems with $x > \frac{1}{4}$, with equilibrium volumes even larger than the PBE predictions.

In summary, we have used high-throughput density functional calculations to map out the low-energy structures in the tungsten nitride system. In general, we find that previously proposed structures, both theoretical and experimental, are not the ground-state structures in this system, with the exception of the "r-W_2N_3" structure. We do find that β-phase structures can be described as various vacancy patterns on the sodium chloride structure, but we cannot explain the experimental preference for tungsten-rich β-phase structures. We also find that none of the density functionals we used correctly describe the system over all compositions, as the LDA and PBE neglect van der Waals forces and the vdW–DF2 functional produces what appear to be spurious predictions for equilibrium structures.

We have also shown that predictions of structural stability must include knowledge of structures over the entire range of compositions. Many of the studies described in Sec. II found structures with negative formation energy ΔH [Eq. (1)], but most of these are not on the convex hull of the tungsten nitride system. One of the structures that is close to the hull, MoS_2, would never have been studied if it were not in the database, as there was no indication that it was likely to occur. The high-throughput mechanism provided by AFLOW is therefore necessary to understand any compound system.

ACKNOWLEDGMENTS

Computational work was done at the U. S. Naval Academy and at the ERDC and AFRL High Performance Computer Centers of the U. S. Department of Defense. We thank Fulton Supercomputing Laboratory and the Cray Corporation for additional computational support. M.J.M. is supported by the Office of Naval Research. D.F. was supported by the Naval Research Laboratory-U. S. Naval Academy Cooperative Program for Scientific Interchange. C.D. was supported by the "Simulation of Materials Under Pressure" Internship at the Naval Research Laboratory. S.C. acknowledges support from DOD-ONR (Grants No. N00014-13-1-0635, No. N00014-11-1 0136, and No. N00014-09-1-0921). G.L.W.H. is grateful for support from the National Science Foundation, Grant No. DMR-0908753. The authors thank Y. Ciftci for providing us with the starting coordinates for the ReP_4 structure used in Ref. [30], J. Wollmershauser for referring us to Ref. [21], and also thank Dr. O. Levy and Dr. A. Stelling for useful comments.

[1] S. Curtarolo, G. L. W. Hart, M. Buongiorno Nardelli, N. Mingo, S. Sanvito, and O. Levy, The high-throughput highway to computational materials design, Nat. Mater. **12**, 191 (2013).

[2] S. M. Woodley and R. Catlow, Crystal structure prediction from first principles, Nat. Mater. **7**, 937 (2008).

[3] *Modern Methods of Crystal Structure Prediction*, edited by A. R. Oganov (Wiley-VCH, Berlin, 2010).

[4] O. Levy, G. L. W. Hart, and S. Curtarolo, Hafnium binary alloys from experiments and first principles, Acta Mater. **58**, 2887 (2010).

[5] G. L. W. Hart and R. W. Forcade, Algorithm for generating derivative structures, Phys. Rev. B **77**, 224115 (2008).

[6] A. R. Oganov, Y. Ma, A. O. Lyakhov, M. Valle, and C. Gatti, in *High Pressure Crystallography: From Fundamental Phenomena to Technological Applications*, NATO Advanced Study Institute, edited by Elena Boldyreva and Przemyslaw Dera (Springer, Dordrecht, The Netherlands, 2010), Chap. 25, pp. 293–323.

[7] X.-L. Sheng, Q.-B. Yan, F. Ye, Q.-R. Zheng, and G. Su, T-Carbon: A novel carbon allotrope, Phys. Rev. Lett. **106**, 155703 (2011).

[8] W. Kohn and L. J. Sham, Self-consistent equations including exchange and correlation effects, Phys. Rev. **140**, A1133 (1965).

[9] P. Hohenberg and W. Kohn, Inhomogeneous electron gas, Phys. Rev. **136**, B864 (1964).

[10] D. M. Ceperley and B. J. Alder, Ground state of the electron gas by a stochastic method, Phys. Rev. Lett. **45**, 566 (1980).

[11] J. P. Perdew and A. Zunger, Self-interaction correction to density-functional approximations for many-electron systems, Phys. Rev. B **23**, 5048 (1981).

[12] J. P. Perdew, K. Burke, and M. Ernzerhof, Generalized gradient approximation made simple, Phys. Rev. Lett. **77**, 3865 (1996).

[13] J. Klimeš, D. R. Bowler, and A. Michaelides, Van der Waals density functionals applied to solids, Phys. Rev. B **83**, 195131 (2011).

[14] G. Hägg, X-ray diffraction investigations on molybdenum and tungsten nitrides, Z. Phys. Chem. B **7**, 339 (1930).

[15] R. Kiessling and Y. H. Liu, Thermal stability of the chromium, iron, and tungsten borides in streaming ammonia and the existence of a new tungsten nitride, J. Metals **3**, 639 (1951).

[16] R. Kiessling and L. Peterson, The nitrides and oxide-nitrides of tungsten, Acta Metall. **2**, 675 (1954).

[17] V. I. Khitrova and Z. G. Pinsker, An electron-diffraction study of cubic tungsten nitride, Kristallografiya **4**, 545 (1959) [Sov. Phys.–Crystallogr. **4**, 513 (1959)].

[18] V. I. Khitrova and Z. G. Pinsker, Chemical crystallography of tungsten nitrides and of some other interesting phases, Kristallografiya **6**, 882 (1962) [Sov. Phys.–Crystallogr. **6**, 712 (1962)].

[19] V. I. Khitrova, WN_2 structure, Kristallografiya **6**, 549 (1961) [Sov. Phys.–Crystallogr. **6**, 439 (1962)].

[20] H.-T. Chiu and S.-H. Chuang, Tungsten nitride thin films prepared by MOCVD, J. Mater. Res. **8**, 1353 (1993).

[21] S. Wang, X. Yu, Z. Lin, R. Zhang, D. He, J. Qin, J. Zhu, J. Han, L. Wang, H.-K. Mao, J. Zhang, and Y. Zhao, Synthesis, crystal structure, and elastic properties of novel tungsten nitrides, Chem. Mater. **24**, 3023 (2012).

[22] H. A. Wriedt, The N-W. (Nitrogen-Tungsten) System, Bull. Alloy Phase Diagrams **10**, 358 (1989).

[23] L. E. Toth, *Transition Metal Carbides and Nitrides* (Academic, New York, London, 1971).

[24] P. Kroll, T. Schröter, and M. Peters, Prediction of novel phases of tantalum(V) nitride and tungsten(VI) nitride that can be synthesized under high pressure and high temperature, Angew. Chem. Int. Ed. **44**, 4249 (2005).

[25] D. V. Suetin, I. R. Shein, and A. L. Ivanovskii, Elastic and electronic properties of hexagonal and cubic polymorphs of tungsten monocarbide WC and mononitride WN from first-principles calculations, Phys. Status Solidi B **245**, 1590 (2008).

[26] H. Wang, Q. Li, Y. Li, Y. Xu, T. Cui, A. R. Oganov, and Y. Ma, Ultra-incompressible phases of tungsten dinitride predicted from first principles, Phys. Rev. B **79**, 132109 (2009).

[27] Y. Benhai, W. Chunlei, S. Xuanyu, S. Qiuju, and C. Dong, Structural stability and mechanical property of WN from first-principles calculations, J. Alloys Compd. **487**, 556 (2009).

[28] X. P. Du, Y. X. Wang, and V. Lo, Investigation of tetragonal ReN2 and WN2 with high shear moduli from first-principles calculations, Phys. Lett. A **374**, 2569 (2010).

[29] L. Song and Y.-X. Wang, First-principles study of W, WN, WN_2, and WN_3, Phys. Status Solidi B **247**, 54 (2010).

[30] S. Aydin, Y. O. Ciftci, and A. Tatar, Superhard transition metal tetranitrides: XN_4 (X. = Re, Os, W), J. Mater. Res. **27**, 1705 (2012).

[31] S. Curtarolo, W. Setyawan, G. L. W. Hart, M. Jahnatek, R. V. Chepulskii, R. H. Taylor, S. Wang, J. Xue, K. Yang, O. Levy, M. Mehl, H. T. Stokes, D. O. Demchenko, and D. Morgan, AFLOW: An automatic framework for high-throughput materials discovery, Comput. Mater. Sci. **58**, 218 (2012).

[32] O. Levy, G. L. W. Hart, and S. Curtarolo, Structure maps for hcp metals from first-principles calculations, Phys. Rev. B **81**, 174106 (2010).

[33] O. Levy, M. Jahnatek, R. V. Chepulskii, G. L. W. Hart, and S. Curtarolo, Ordered structures in rhenium binary alloys from first-principles calculations, J. Am. Chem. Soc. **133**, 158 (2011).

[34] M. Jahnatek, O. Levy, G. L. W. Hart, L. J. Nelson, R. V. Chepulskii, J. Xue, and S. Curtarolo, Ordered phases in ruthenium binary alloys from high-throughput first-principles calculations, Phys. Rev. B **84**, 214110 (2011).

[35] O. Levy, J. Xue, S. Wang, G. L. W. Hart, and S. Curtarolo, Stable ordered structures of binary technetium alloys from first principles, Phys. Rev. B **85**, 012201 (2012).

[36] G. L. W. Hart, S. Curtarolo, T. B. Massalski, and O. Levy, Comprehensive search for new phases and compounds in binary alloy systems based on platinum-group metals, using a computational first-principles approach, Phys. Rev. X **3**, 041035 (2013).

[37] S. Curtarolo, W. Setyawan, S. Wang, J. Xue, K. Yang, R. H. Taylor, L. J. Nelson, G. L. W. Hart, S. Sanvito, M. Buongiorno Nardelli, N. Mingo, and O. Levy, AFLOWLIB.ORG: A distributed materials properties repository from high-throughput *ab initio* calculations, Comput. Mater. Sci. **58**, 227 (2012).

[38] M. Dion, H. Rydberg, E. Schröder, D. C. Langreth, and B. I. Lundqvist, Van der Waals density functional for general geometries, Phys. Rev. Lett. **92**, 246401 (2004).

[39] M. Born, On the stability of crystal lattices. I, Proc. Cambridge Philos. Soc. **36**, 160 (1940).

[40] J. Donohue, *The Structures of the Elements* (Wiley, New York, 1974), Chap. 8, pp. 280–288.

[41] J. Donohue, *The Structures of the Elements* (Wiley, New York, 1974), Chap. 6, pp. 187–191.

[42] C. B. Barber, D. P. Dobkin, and H. Huhdanpaa, The quickhull algorithm for convex hulls, ACM Trans. Math. Software **22**, 469 (1996).

[43] *Strukturbericht 1913-1928*, Vol. I, edited by P. P. Ewald and K. Herman (Akademische Verlagsgesellschaft M. B. H., Leipzig, 1931).

[44] W. B. Pearson, *The Crystal Chemistry and Physics of Metals and Alloys* (Wiley-Interscience, New York, 1972).

[45] J. Donohue, *The Structures of the Elements* (Wiley, New York, 1974).

[46] *Pearson's Handbook of Crystallographic Data for Intermetallic Phases*, edited by P. Villars and L. D. Calvert, 2nd ed. (ASM International, Materials Park, Ohio, 1991).

[47] R. T. Downs and M. Hall-Wallace, The *American Minerologist* crystal structure database, Am. Mineral. **88**, 247 (2003).

[48] See Supplemental Material at http://link.aps.org/supplemental/10.1103/PhysRevB.91.184110 which a complete crystallographic description and equilibrium configuration of all the structures discussed in this paper.

[49] N. Schönberg, Contributions to the knowledge of the molybdenum-nitrogen and the tungsten-nitrogen systems, Acta Chem. Scand. **8**, 204 (1954).

[50] Y. G. Shen and Y. W. Mai, Structural studies of amorphous and crystallized tungsten nitride thin films by EFED, XRD and TEM, Appl. Surf. Sci. **167**, 59 (2000).

[51] W. B. Pearson, *The Crystal Chemistry and Physics of Metals and Alloys* (Wiley-Interscience, New York, 1972), Chap. 8, pp. 452–454.

[52] T. Siegrist and F. Hulliger, High-temperature behavior of $CoAs_2$ and $CoSb_2$, J. Solid State Chem. **63**, 23 (1896).

[53] E. P. Meagher and G. A. Lager, Polyhedral thermal expansion in the TiO_2 polymorphs: Refinement of the crystal structures

of rutile and brookite at high temperature, Canadian Mineral. **17**, 77 (1979).

[54] R. W. G. Wyckoff (ed.), *Crystal Structures* (Wiley, New York, 1963), Vol. I, pp. 298–306.

[55] R. Hill, The elastic behaviour of a crystalline aggregate, Proc. Phys. Soc. A **65**, 349 (1952).

[56] R. Rühl and W. Jeitschko, Preparation and structure of technetium triphosphide and rhenium triphosphide, isotypic polyphosphides with metal chains, Acta Crystallogr. B **38**, 2784 (1982).

[57] D. V. Suetin, I. R. Shein, and A. L. Ivanovskii, Electronic structure of cubic tungsten subnitride W_2N. in comparison to hexagonal and cubic tungsten mononitrides WN, J. Struct. Chem. **51**, 199 (2010).

[58] H. Goretzki, Neutron diffraction studies on titanium-carbon and zirconium-carbon alloys, Phys. Status Solidi **20**, K141 (1967).

[59] L. Xiao-Feng, Z. Hong-Cun, F. Hong-Zhi, L. Zhong-Li, and J. Guang-Fu, Physical properties of hexagonal WN_2 under pressure, Chinese Phys. B **20**, 093101 (2011).

[60] *Strukturbericht 1913-1928*, edited by P. P. Ewald and K. Herrman (Akademische Verlagsgesellschaft M. B. H., Leipzig, 1931), Vol. I, pp. 76–77.

[61] R. F. Zhang, Z. J. Lin, H.-K. Mao, and Y. Zhao, Thermodynamic stability and unusual strength of ultra-incompressible rhenium nitrides, Phys. Rev. B **83**, 060101 (2011).

[62] R. F. Zhang, S. Veprek, and A. S. Argon, Anisotropic ideal strengths and chemical bonding of wurtzite BN in comparison to zincblende BN, Phys. Rev. B **77**, 172103 (2008).

[63] W. Jeitschko and R. Rühl, Synthesis and crystal structure of diamagnetic ReP_4, a polyphosphide with Re-Re pairs, Acta Crystallogr., Sect. B: Struct. Crystallogr. Cryst. Chem. **35**, 1953 (1979).

[64] M. Zhang, H. Yan, Q. Wei, and H. Wang, Mechanical and electronic properties of novel tungsten nitride, Europhys. Lett. **100**, 46001 (2012).

[65] M. Zumbusch, Über die Strukturen des Uransubsulfids und der Subphosphide des Iridiums und Rhodiums, Z. Anorg. Allg. Chem. **243**, 322 (1940).

[66] K. Liu, S.-M. Wang, X.-L. Zhou, and J. Chang, Theoretical calculations for structural, elastic, and thermodynamic properties of c-W_3N_4 under high pressure, J. Appl. Phys. **114**, 063512 (2013).

[67] Z. Liu, X. Zhou, D. Gall, and S. Khare, First-principles investigation of the structural, mechanical and electronic properties of the NbO-structured 3d, 4d and 5d transition metal nitrides, Comput. Mater. Sci. **84**, 365 (2014).

[68] R. W. G. Wyckoff, *Crystal Structures*, Vol. I, 2nd ed. (Wiley, New York, 1963).

[69] P. Villars and L. D. Calvert, *Pearson's Handbook of Crystallographic Data for Intermetallic Phases*, 2nd ed. (ASM International, Materials Park, Ohio, 1991), Vol. 4, pp. 4759–4763.

[70] A. V. D. Geest and A. Kolmogorov, Stability of 41 metal-boron systems at 0 GPa and 30 GPa from first principles, Calphad **46**, 184 (2014).

[71] R. H. Taylor, F. Rose, C. Toher, O. Levy, K. Yang, M. Buongiorno Nardelli, S. Curtarolo, and A. RESTful, API for exchanging Materials Data in the AFLOWLIB.org consortium, Comput. Mater. Sci. **93**, 178 (2014).

[72] G. Kresse and J. Hafner, *Ab initio* molecular dynamics for open-shell transition metals, Phys. Rev. B **48**, 13115 (1993).

[73] G. Kresse and J. Hafner, *Ab initio* molecular-dynamics simulation of the liquid-metal/amorphous-semiconductor transition in germanium, Phys. Rev. B **49**, 14251 (1994).

[74] G. Kresse and D. Joubert, From ultrasoft pseudopotentials to the projector augmented-wave method, Phys. Rev. B **59**, 1758 (1999).

[75] P. E. Blöchl, Projector augmented-wave method, Phys. Rev. B **50**, 17953 (1994).

[76] M. I. Eremets, R. J. Hemley, H.-K. Mao, and E. Gregoryanz, Semiconducting non-molecular nitrogen up to 240 GPa and its low-pressure stability, Nature (London) **411**, 170 (2001).

[77] J. Klimeš, D. R. Bowler, and A. Michaelides, Chemical accuracy for the van der Waals density functional, J. Phys.: Condens. Matter **22**, 022201 (2010).

[78] H. J. Monkhorst and J. D. Pack, Special points for Brillouin-zone integrations, Phys. Rev. B **13**, 5188 (1976).

[79] MedeA® is a registered trademark of Materials Design Inc.

[80] M. J. Mehl, J. E. Osburn, D. A. Papaconstantopoulos, and B. M. Klein, Structural properties of ordered high-melting-temperature intermetallic alloys from first-principles total-energy calculations, Phys. Rev. B **41**, 10311 (1990); **42**, 5362(E) (1990).

[81] M. J. Mehl, B. M. Klein, and D. A. Papaconstantopoulos, First-principles calculation of elastic properties, in *Intermetallic Compounds - Principles and Practice*, edited by J. H. Westbrook and R. L. Fleischer (Wiley, London, 1995), Vol. 1, Chap. 9, pp. 195–210.

[82] G. Kresse, *Ab initio Molekular Dynamik für flüssige Metalle*, Ph.D. thesis, Technische Universität Wien, Vienna, 1993.

[83] R. L. Mills, B. Olinger, and D. T. Cromer, Structures and phase diagrams of N_2 and CO to 13 GPa by x-ray diffraction, J. Phys. Chem. **84**, 2837 (1986).

[84] H. L. Yu, G. W. Yang, X. H. Yan, Y. Xiao, Y. L. Mao, Y. R. Yang, and M. X. Cheng, First-principles calculations of the single-bonded cubic phase of nitrogen, Phys. Rev. B **73**, 012101 (2006).

[85] C. Kittel, *Introduction to Solid State Physics*, 7th ed. (Wiley, New York, 1996).

[86] F. Birch, Finite strain isotherm and velocities for single-crystal and polycrystalline nacl at high-pressures and 300-degree-k, J. Geophys. Res. **83**, 1257 (1978).

[87] VASP includes a mode which determines the equilibrium structure by minimizing the pressure. However, pressure is not a variational quantity, and N_2 is a soft crystal, meaning that small errors in the pressure can produce large errors in the equilibrium volume. The error will indeed decrease with increasing numbers of plane waves, but it is much easier to determine the equilibrium configuration by direct calculation.

[88] Z. Hashin and S. Strikman, On some variational principles in anisotropic and nonhomogeneous elasticity, J. Mech. Phys. Solids **10**, 335 (1962).

[89] Z. Hashin and S. Shtrikman, A. variational approach to the theory of the elastic behavior of polycrystals, J. Mech. Phys. Solids **10**, 343 (1962).

[90] D. A. Evans and K. H. Jack, The $\gamma \rightarrow \beta$ phase transformation in the Mo-N. system, Acta Crystallogr. **10**, 833 (1957).

[91] M. Lax, *Symmetry Principles in Solid State and Molecular Physics* (Wiley, New York, 1974).

[92] W. Setyawan and S. Curtarolo, High-throughput electronic band structure calculations: Challenges and tools, Comput. Mater. Sci. **49**, 299 (2010).

[93] W. B. Pearson, *The Crystal Chemistry and Physics of Metals and Alloys* (Wiley-Interscience, New York, 1972), Chap. 7, pp. 309–310.

[94] *Strukturbericht 1913-1928*, edited by P. P. Ewald and K. Herrman (Akademische Verlagsgesellschaft M. B. H., Leipzig, 1931), Vol. I, pp. 166–169.

[95] P. Woodward, Structures based on linked polyhedra, Http://chemistry.osu.edu/∼woodward/ch754/str_poly.htm

[96] K. Kihara, Thermal change in unit-cell dimensions, and a hexagonal structure of tridymite, Z. Kristallogr. **148**, 237 (1975).

[97] H. Dachs, Die Kristallstruktur des Bixbyits (Fe, Mn)$_2$O$_3$, Z. Kristallogr. **107**, 370 (1956).

[98] W. Zachariasen, XXXI. Über die Kristallstruktur von Bixbyit, sowie vom künstlichen Mn_2O_3, Z. Kristallogr. **67**, 455 (1928). As quoted in the American Mineralogist Crystal Structure Database, http://rruff.geo.arizona.edu/AMS/amcsd.php

[99] H.-J. Schweizer and R. Gruehn, Synthesis and Crystal Structure of β-NbO_2, Z. Naturforsch. B **37**, 1361 (1982).

[100] R. J. Hill, The crystal structures of lead dioxides from the positive plate of the lead/acid battery, Mater. Res. Bull. **17**, 769 (1982).

[101] *Strukturbericht 1913-1928*, edited by P. P. Ewald and K. Herrman (Akademische Verlagsgesellschaft M. B. H., Leipzig, 1931), Vol. I, pp. 164–166.

[102] B. Schönfeld, J. J. Huang, and S. C. Moss, Anisotropic mean-square displacements (MSD) in single-crystals of 2H- and 3R-MoS_2, Acta Crystallogr. B **39**, 404 (1983).

[103] G. Andersson and A. Magnéli, On the crystal structure of molybdenum trioxide, Acta Chem. Scand. **4**, 793 (1950).